THE ASTROPHYSICAL JOURNAL, 494:342–365, 1998 February 10

A PRECISION VELOCITY STUDY OF PHOTOMETRICALLY STABLE STARS IN THE CEPHEID INSTABILITY STRIP[1]

R. PAUL BUTLER[2,3]
Department of Physics and Astronomy, San Francisco State University, San Francisco, CA 94132; paul@aaoepp.aao.gov.au
Received 1997 May 21; accepted 1997 September 17

ABSTRACT

Results of a precision Doppler velocity survey of 15 stars that lie in or near the Cepheid instability strip are presented. Previous studies have shown that these stars are photometrically stable. Long-term radial velocity precision of 15 m s^{-1} has been achieved with the use of an iodine absorption cell and a high-resolution cross-dispersed echelle spectrometer. The stars show a variety of behavior from stability (at the level of 30 m s^{-1}) to variability from 50 m s^{-1} to a few km s^{-1}. Periodograms of many of the program stars show significant peaks at 50–80 days that are not associated with radial pulsation. Previously undetected binary companions have been found around two of the stars. Line profiles are compared to δ Cep.

Subject headings: binaries: spectroscopic — Cepheids — stars: oscillations — techniques: radial velocities

1. INTRODUCTION

A number of photometric studies have shown that at least one-half of the stars that reside in the Cepheid region of the instability strip are photometrically stable at the level of 0.01–0.03M_V (Fernie & Hube 1971; Schmidt 1972; Percy 1975; Fernie 1976; Percy, Baskerville, & Trevorrow 1979). Studies of these stars have broad implications for several theoretical and observational aspects of Cepheid variable stars.

After seven decades of intensive study, a number of outstanding questions remain unanswered about Cepheids. The radial velocity amplitude of Cepheids with similar color and period can differ by more than an order of magnitude. It is not known what sets the radial velocity amplitude, or why nonvariable stars exist in the instability strip. The boundaries of the Cepheid instability strip are not well known. It has recently been suggested that the instability strip is much narrower than has traditionally been thought (Fernie 1990; Chiosi et al. 1992).

Historically, small-amplitude variables have been discovered because of their photometric variations. Over the last decade, observational advances have improved the precision of Doppler velocity measurements by 2 orders of magnitude, from 500 to 3 m s^{-1}. Precision velocity techniques are now exquisitely sensitive to small amplitude variations. Recent precision velocity studies have found that K giants undergo radial velocity variations of 25–300 m s^{-1} with periods ranging from hours to years (Smith, McMillan, & Merline 1987; Walker et al. 1989; Larson et al. 1993; Hatzes & Cochran 1993, 1994). Other recent studies have found that F and G supergiants vary by $\sim$100 m s^{-1} (Butler 1992; Hatzes & Cochran 1995).

This paper presents the results of a 6 yr survey of 15 photometrically stable stars that lie in or near the Cepheid instability strip. The observational technique and stellar sample are described in § 2. The Doppler velocity results and preliminary analysis are presented in § 3. Line profiles are examined in § 4, including a comparison with δ Cep. A discussion of the results follows in § 5.

2. OBSERVATIONAL TECHNIQUE AND STELLAR SAMPLE

All of the observations presented in this paper were taken at Lick Observatory with the Hamilton, a cross-dispersed coudé echelle spectrometer (Vogt 1987). The Hamilton is fed by both the 0.6 m Coudé Auxiliary Telescope (CAT) and the 3 m Shane Telescope. Most of the observations reported in this paper were made with the CAT.

High-precision Doppler velocity measurements have been made via the iodine absorption cell technique (Butler et al. 1996; Valenti, Butler, & Marcy 1995; Marcy & Butler 1992). In brief, wavelength calibration is accomplished by placing an iodine gas absorption cell directly in front of the spectrometer slit. Starlight thus passes through the iodine absorption cell before entering the spectrometer. The superposed absorption lines of iodine serve as indelible wavelength markers, and their shapes convey the local spectrometer point-spread function (PSF). The wavelength and PSF parameters are determined by constructing a model of the spectrum, which includes the unknown Doppler shift. Relative Doppler errors were $\sim$15 m s^{-1} until 1994 November, when improvements in the spectrometer brought the errors down to 3 m s^{-1}. A number of stable stars are shown in Figure 1 of Marcy & Butler (1996), Figure 2 of Butler & Marcy (1996), and Figures 3 and 4 of Butler & Marcy (1997).

The 15 stars listed in Table 1 have been monitored for 4–8 yr each. These stars are among the brightest apparently stable stars that lie in or near the Cepheid instability strip (Hoffleit & Jaschek 1982) and can be accessed by the 0.6 m Coudé Auxiliary Telescope at Lick Observatory in the summer months. Eleven of these stars were previously surveyed by Burki & Mayor (1983) at a precision of 300–400 m s^{-1} using CORAVEL. With one exception, HR 1884, these stars were found to be stable. Nine of the program stars have been photometrically monitored by Fernie & Hube (1971) and Fernie (1976). Photometric variations ranged from less than 0.005 to 0.03 mag. Fernie (1976) writes that

[1] Based on observations obtained at Lick Observatory, operated by the University of California.
[2] Also at Department of Astronomy, University of California, Berkeley, CA 94720.
[3] Current address: Anglo-Australian Observatory, P.O. Box 296, Epping NSW 2121, Australia.

TABLE 1

STELLAR SAMPLE

Star	Name	HD	M_V	Spectral Type
HR 157	...	HD 3421	5.48	G2.5IIa
HR 213	58 Psc	HD 4482	5.50	G8II
HR 461	...	HD 9900	5.56	G5II
HR 800	14 Per	HD 16901	5.43	G0Ib-II
HR 1017.....	α Per	HD 20902	1.79	F5Ib
HR 1603.....	β Cam	HD 31910	4.03	G0Ib
HR 1884.....	...	HD 36891	6.09	G3Ib
HR 6536.....	β Dra	HD 159181	2.79	G2Ib-IIa
HR 6978.....	45 Dra	HD 171635	4.77	F7Ib
HR 7387.....	32 ν Aql	HD 182835	4.66	F2Ib
HR 7796.....	γ Cyg	HD 194093	2.20	F8Ib
HR 7834.....	41 Cyg	HD 195295	4.01	F5II
HR 8232.....	β Aqr	HD 204867	2.91	G0Ib
HR 8313.....	9 Peg	HD 206859	4.34	G5Ib
HR 8414.....	α Aqr	HD 209750	2.96	G2Ib

"none of these variations could be assembled into a convincing light curve, and are taken to be just the irregular variability accepted as normal in supergiants."

The stars in this program span the spectral range from F2Ib though G5Ib, along with a handful of F and G type II stars. An H-R diagram of the program stars is shown in Figure 1, along with the boundaries of the Cepheid instability strip. The approximate boundaries of the "restricted" Cepheid instability strip (Fernie 1990; Chiosi et al. 1992) are indicated by the solid lines, while a more traditional red edge of the instability strip is indicated by the dashed line. Although there is significant uncertainty in the determination of absolute magnitudes, this figure demonstrates that most of the program stars lie in or at least very near to the instability strip.

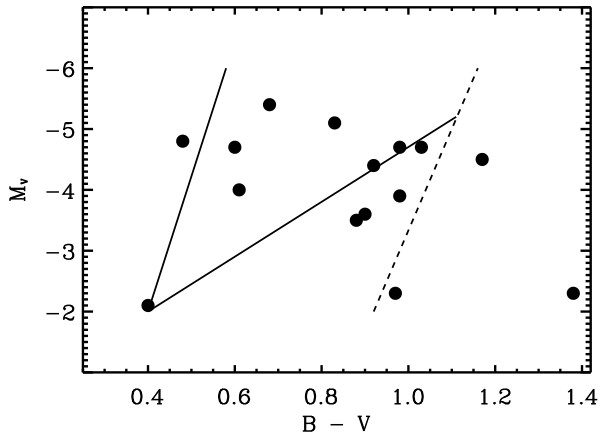

FIG. 1.—H-R diagram of the program stars. Solid lines indicate the "restricted instability strip" of Fernie (1990), while the dotted line shows a more traditional red edge. Though the absolute magnitudes of the program stars are uncertain by ~1, most of these stars lie either in or near the instability strip.

3. DOPPLER VELOCITY RESULTS

The Doppler velocity measurements of the program stars are presented here, along with preliminary analysis. Each star has been observed about 50 times over 4–6 yr. The stars were typically observed on consecutive nights for 1 or 2 weeks during the summer and/or fall from 1991 through 1995. A few stars have been observed for up to 8 yr.

Scargle (1982) periodogram analysis, similar to that described in Gilliland & Baliunas (1987), is employed in searching for periodicities in the data. The significance of the periodogram peaks has been determined by Monte Carlo simulations. The measured Doppler velocities were randomly reassigned to the observation dates, and periodograms of the resulting scrambled velocity sets were determined. A total of 500 trials of each star were run in order to find the level at which the peaks were significant at the 1% level (Murdoch, Hearnshaw, & Clark 1993). Table 2 lists the number of observations of each star, the median internal measurement error (σ_{INT}), the rms of the measured Doppler velocities (σ_{EXT}), the most probable period from periodogram analysis, the rms of the sine fit to the measured velocities at the most probable period (σ_{SIN}), and the semi-amplitude (K_{SIN}) of the sinusoidal fit.

Two of the stars, HR 213 and HR 1884, have Doppler variations that are consistent with orbiting stellar companions. The Keplerian orbital parameters for these stars are given in Table 3. Less than one-half of the orbit has been observed for HR 1884, leaving the derived orbital parameters quite uncertain. The individual velocity measurements for all the program stars are given in Tables 4–18.

All of the stars show Doppler velocity variations in excess of measurement error. Periodograms reveal significant periodicities for all of the stars. Many of these periodograms

TABLE 2

SUMMARY OF OBSERVATIONS

Star	Number of Observations	σ_{INT} (m s^{-1})	σ_{EXT} (m s^{-1})	Period (days)	σ_{SIN} (m s^{-1})	K_{SIN} (m s^{-1})
HR 157	32	11.4	33.0	15.198	24.9	35.5
HR 213	34	9.7	24.5[a]	...	...	...
HR 461	31	10.0	92.8	69.180	49.7	139.6
HR 800	61	17.6	79.0	51.026	58.9	102.0
HR 1017.....	63	17.3	100.8	77.717	56.2	108.9
HR 1603.....	47	13.2	63.4	44.717	46.5	67.0
HR 1884.....	42	17.0	90.7[a]	...	...	...
HR 6536.....	41	5.4	50.3	21.292	37.3	58.1
HR 6978.....	48	11.0	36.1	79.708	27.4	36.0
HR 7387.....	64	55.3	947.9	84.126	544	819
HR 7796.....	105	16.4	536.7	74.440	353	554
HR 7834.....	51	12.5	23.8	70.674	17.5	21.7
HR 8232.....	70	10.5	154.5	203.42	98.8	219
HR 8313.....	52	12.9	83.6	230.91	62.5	92.5
HR 8414.....	86	11.5	122.8	76.152	87.1	126.1

[a] After removing Keplerian orbital fit.

TABLE 3

BINARY ORBITAL PARAMETERS

Parameter	HR 213	HR 1884[a]
P (d)	843 (4)	9390
T_p (JD)	2449602.12 (3.5)	2448591.9
e	0.386 (0.013)	0.896
ω^2 (deg)	219.6 (0.6)	253
K_1 (m s^{-1}).....	5277 (10)	21877
$a_1 \sin i$ (AU).....	0.377	8.38
f_1(m) ($M_\odot$)	0.0101	0.89
O-C (m s^{-1})	33.3	90.7

[a] Only ~25% of the orbit has been observed.

bear a "family resemblance" with primary or secondary peaks of 50–80 days. Often, there are two or three strong aliased peaks, resulting from uneven data sampling. The problem of periodogram aliasing is studied with a Monte Carlo simulation of the data. A sine is fitted to the data at each of the preferred periods, and the rms of the sine fit is noted. A model of the data is constructed by adding random noise with an appropriate rms to the sinusoidal fit. The window function is maintained by sampling the "noisy sinusoids" at the times of the observations. A hundred such models are constructed, and periodograms are determined for each of the resulting models. The periods of the four highest peaks in each of the model data periodograms are stored, then compared to the highest peaks from the periodogram of the original data.

3.1. *HR 157* (*G2.5IIa*)

The Doppler velocity measurements for HR 157 are shown in Figure 2. This is one of the most stable stars in the program. The rms of the measured velocities is 33 m s^{-1}, only 3 times larger than measurement error. A periodogram analysis of these velocities finds weak periodicities at 6 and 15 days—the shortest period of all the program stars.

3.2. *HR 213* (*G8II*)

The Doppler velocities of HR 213, shown in Figure 3 (*top*), reveal a binary companion. The orbital fit is shown as a solid line. The rms of the residuals to the orbital fit (Fig. 3, *bottom*) are 33 m s^{-1}. The orbital parameters are given in Table 3. The period is 843 days, the eccentricity is 0.386, and the semi-amplitude is 5277 m s^{-1}. The Bright Star Catalog does not indicate that HR 213 is part of a binary or multiple system. Assuming that HR 213 has a mass of ~5 $M_\odot$ (based on spectral type), the companion would have a minimum mass $m \sin i$ of 0.6 $M_\odot$ and a semimajor axis of 3 AU. A periodogram of the residual velocities after subtracting the orbital fit finds weak periodicities at 5 yr and 16 days.

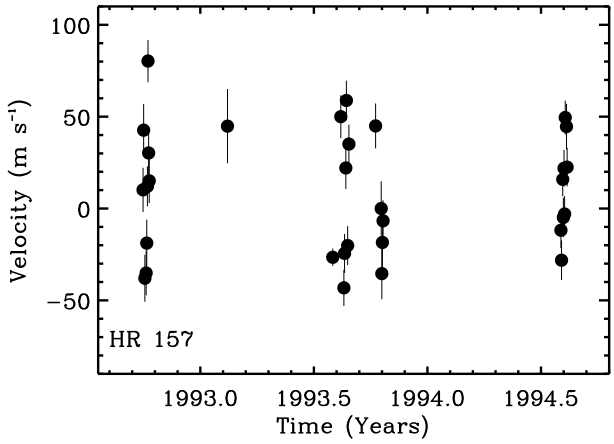

FIG. 2.—Measured Doppler velocities of HR 157. The rms of the measured velocities is 33 m s^{-1}, 3 times larger than measurement error. This is among the most stable of the program stars.

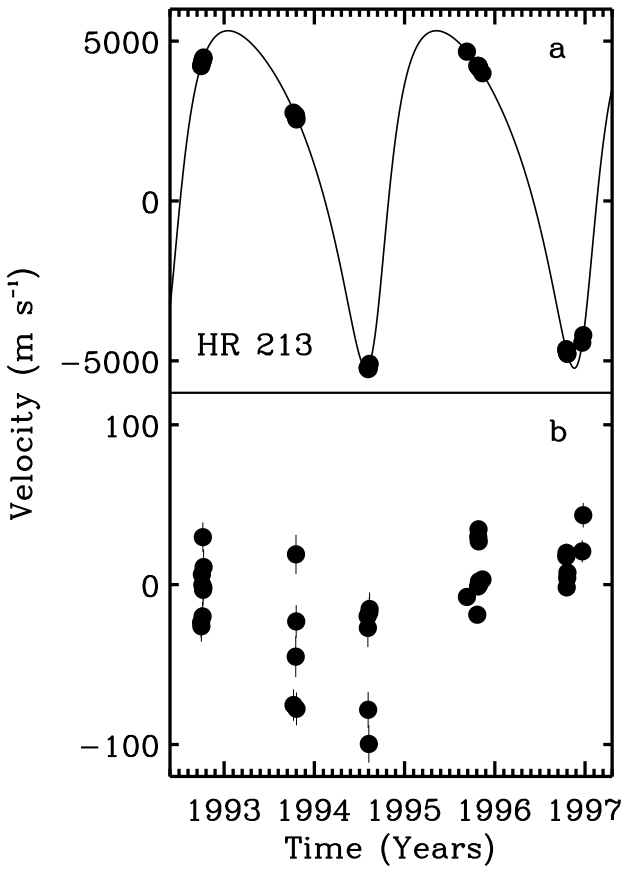

FIG. 3.—HR 213 Doppler velocities. (*a*) Measured Doppler velocities, spanning slightly more than 4 yr, reveal the presence of an orbiting companion. The solid line is a Keplerian fit to the velocities. The orbital period is 843 days, the semi-amplitude is 5277 m s^{-1}, and the eccentricity is 0.386. Assuming that the primary has a mass of 5 $M_\odot$ (consistent with spectral type), the companion has a minimum (m sin i) mass of 0.6 $M_\odot$ and a semimajor axis of 3 AU. (*b*) Residual velocities, after subtracting the Keplerian fit. The rms of the residuals is 24.5 m s^{-1}.

3.3. *HR 461* (*G5II*)

The measured Doppler velocities for HR 461 are shown in Figure 4. The uncertainty of the individual measurements is typically 10 m s^{-1}. The rms of the full data set is 93 m s^{-1}, while the scatter within each of the observing seasons is about 50 m s^{-1}.

A periodogram of the velocities (Fig. 5*a*) reveals a strong peak at 69.180 days. Figure 6 shows the velocities phased with this period. The sinusoid fit (*solid line*) to the phased velocities has a rms of 50 m s^{-1}. The semi-amplitude of the sine is 140 m s^{-1}. Figure 5*b* shows a periodogram of the HR 461 velocities with the sinusoid subtracted. The peaks seen near 400 and 900 days in the original periodogram (Fig. 5*a*) fall well below the 1% false alarm level. The remaining peaks are weak, barely reaching the 1% false alarm level, with periods of less than 20 days.

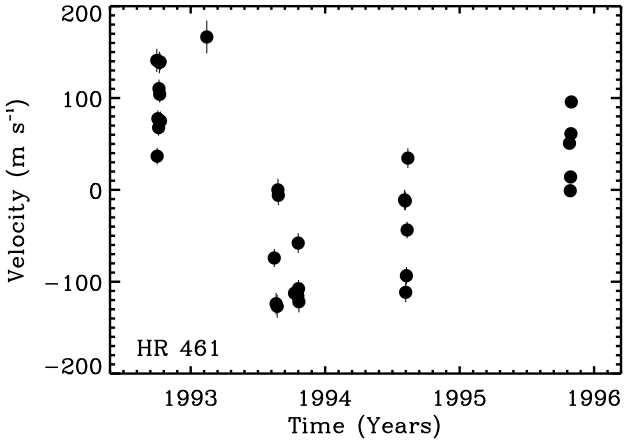

FIG. 4.—Measured Doppler velocities of HR 461. The rms scatter of the velocities is 93 m s^{-1}. Measure errors are typically 10 m s^{-1}.

3.4. *HR 800 (G0Ib-II)*

The measured Doppler velocities for HR 800 are shown in Figure 7. The full amplitude of the velocity variations is $\sim$250 m s^{-1}. The rms of the measured velocities is 79 m s^{-1}, while typical measurement error is 18 m s^{-1}. The velocities appear to drop from 1991 through 1993, and then begin increasing, suggesting a possible $\sim$10 yr period.

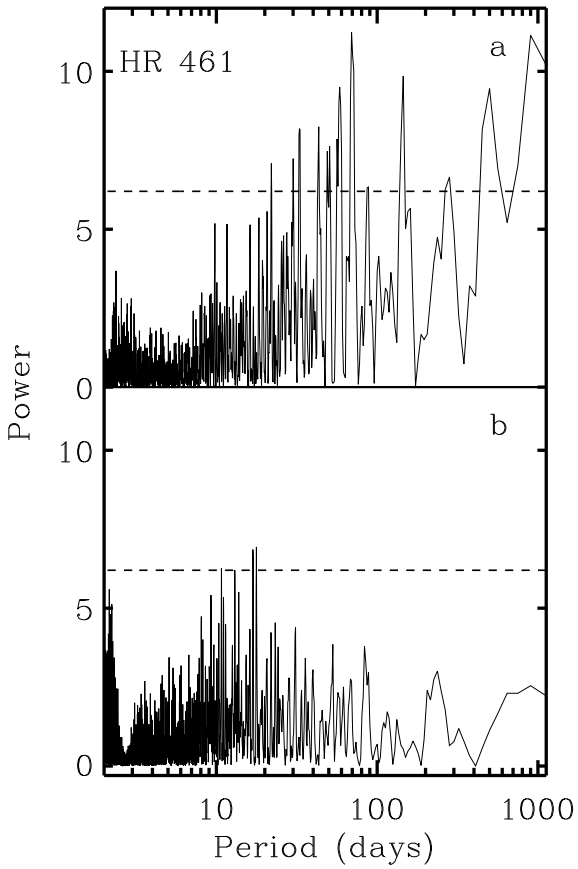

FIG. 5.—Periodogram of HR 461 velocities. (*a*) Periodogram of measured velocities. The periodogram peaks at 69.180 days, with a number of secondary peaks at much longer periods. The 1% false alarm level is indicated by the dashed line. (*b*) Periodogram of residual velocities, after subtracting a best-fit sinusoid with a period of 69.180 days. The remaining periodogram peaks are significantly decreased. The long-period peaks seen in Fig. 5*a* essentially disappear.

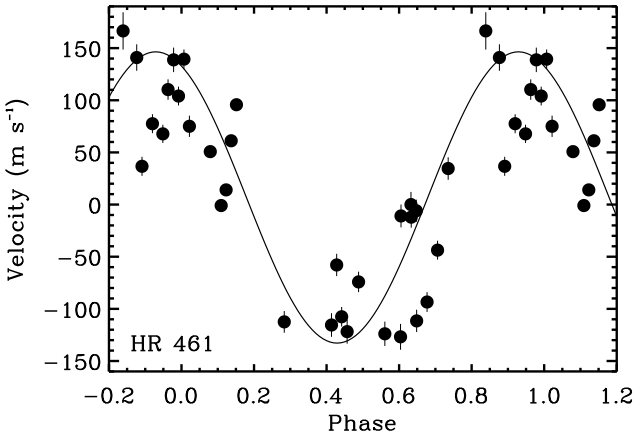

FIG. 6.—HR 461 velocities phased with a period of 69.180 days. The rms to the sinusoidal fit is 49.7 m s^{-1}.

The periodogram (Fig. 8*a*) shows peaks at 491.5, 51.0, and 293.9 days. These peaks are probably aliases. In Figure 9 the observed velocities are phased with the periods of the two highest peaks from the periodogram. Figure 9*a* shows the data phased with the 491.5 day period, while Figure 9*b* has the data phased with the 51.0 day period. The rms of the residuals to the sinusoidal fit for the 491.5 day period is 53.8 m s^{-1}, while the rms of the residuals to the 51.0 day fit is 58.9 m s^{-1}.

A hundred sinusoidal models of the data have been constructed at each of the two peak periods found from the periodogram. Random noise with a rms of 55 m s^{-1} was added to the sinusoids, and they were then sampled at the times of the observations to take into account the window function. Periodograms were run on resulting model velocities. For the case of the 491.5 day sinusoid, 87% of the periodograms found a periodicity of between 50 and 52 days, while 6% of the periodograms found a period between 278 and 308 days. For the 51 day sinusoid, periodicities between 476 and 506 days were found in 37% of the periodograms, and 52% of the periodograms found periodicities between 278 and 308 days. Thus, both a 491.5 and a 51.0 day periodicity can account for all observed peak periodicities, although the 51.0 day periodicity is more likely to account for the 293.9 day peak.

The star was repeatedly observed for 10 or more nights on three different observing runs. The results are shown in

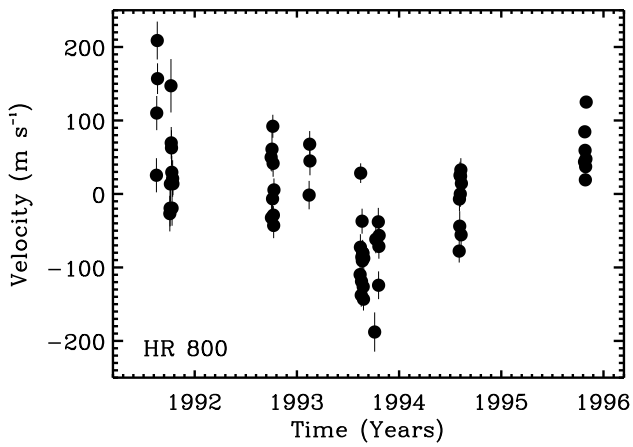

FIG. 7.—Measured Doppler velocities for HR 800. The rms is 79 m s^{-1}.

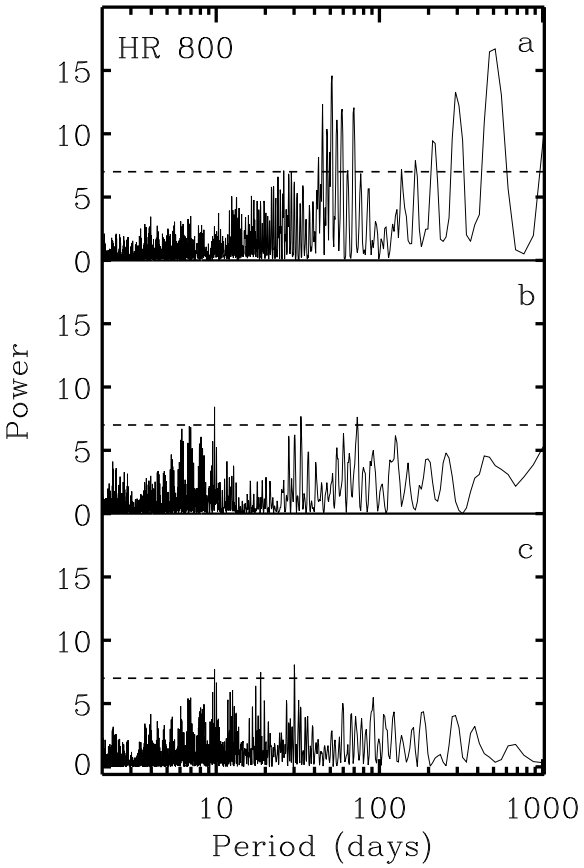

FIG. 8.—Periodogram of HR 800 velocities. (*a*) Periodogram of measured velocities. The three highest periodogram peaks have periodicities of 491.5, 51.0, and 293.9 days. The 1% false alarm level is indicated by the dotted line. (*b*) Periodogram of residual velocities, after subtracting a best-fit sinusoid with a period of 491.5 days. The remaining periodogram peaks are significantly decreased. (*c*) Periodogram of residual velocities, after subtracting a best-fit sinusoid with a period of 51.0 days. The remaining periodogram peaks are significantly decreased.

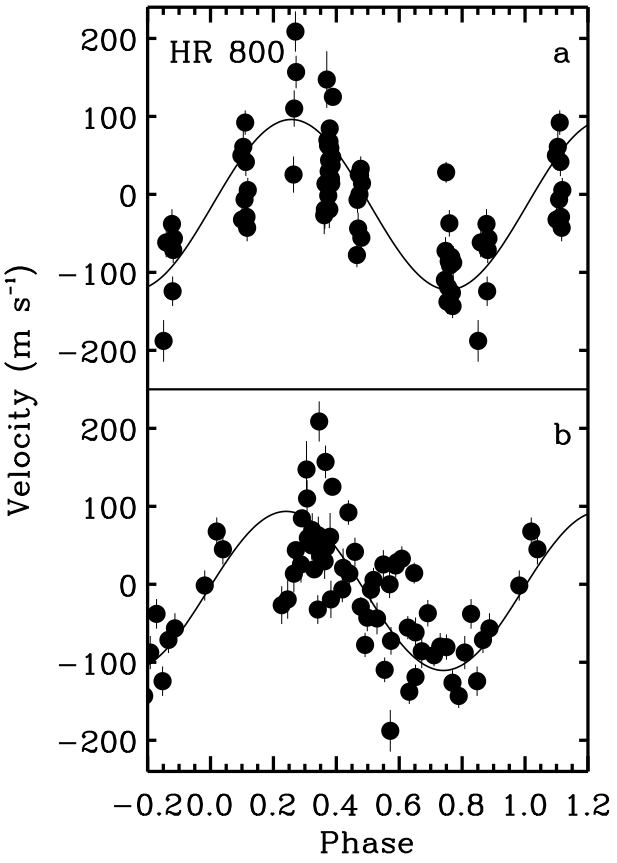

FIG. 9.—Phased Doppler velocities for HR 800. (*a*) Doppler velocities phased with a 491.483 day period. The rms to the sinusoidal fit is 54 m s^{-1}. (*b*) Doppler velocities phased with a 51.026 day period. The rms to the sinusoidal fit is 59 m s^{-1}.

Figure 10. The velocity zero point of each of the observing runs is arbitrary. The circles are from an observing run that began in 1991 early October, and they span 11 nights. The squares are from 1992 late September and span 10 nights. The diamonds are from 1993 mid-August and span 13 nights. On several occasions the velocity of the star is seen to change by $\sim$150 m s^{-1} over 1–3 days. The full amplitude of the velocity variations seen in Figure 7 is only $\sim$250 m s^{-1}, suggesting that the longer periods (293.9 and 491.5 days) seen in the periodogram are the aliased periods.

A periodogram of the residual velocities, after subtracting the 491.5 day sinusoid, is shown in Figure 8*b*, while Figure 8*c* shows the periodogram of the residuals after subtracting the 51.0 day sinusoid.

3.5. *HR 1017 (F5Ib)*

Doppler velocity variability in HR 1017 was first reported by Hatzes & Cochran (1995), based on 24 observations made between 1991 October and 1993 August. A total of 63 observations made between 1991 August and 1995 October are shown in Figure 11. The rms of the measured velocities is 101 m s^{-1}, while the full amplitude of the velocity variations is $\sim$350 m s^{-1}, in agreement with Hatzes & Cochran.

A periodogram of these velocities is shown in Figure 12*a*. A single dominant period is seen at 77.717 days. In contrast, Hatzes & Cochran report possible periodicities of 87.7 and 9.8 days. Figure 13 shows 14 observations of HR 1017 taken over 25 nights, beginning in 1993 early August. The velocities are seen to increase by 220 m s^{-1} over this interval, ruling out the 9.8 day periodicity. The velocities are phased

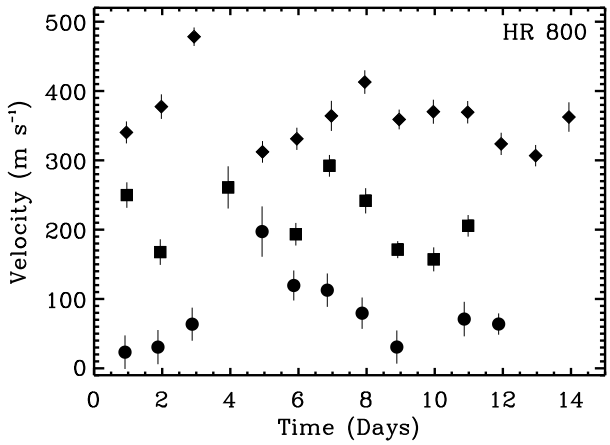

FIG. 10.—Nightly velocity variations of HR 800 from three observing runs. The velocity zero point of each of these runs is arbitrary. *Circles:* Observing run that began in 1991 early October; *squares:* observing run that began in 1992 late September; *diamonds:* observing run that began in 1993 August. Velocity variations within a single run are typically $\sim$150 m s^{-1}, about one-half of the full range of variation seen over the 4 yr observing span.

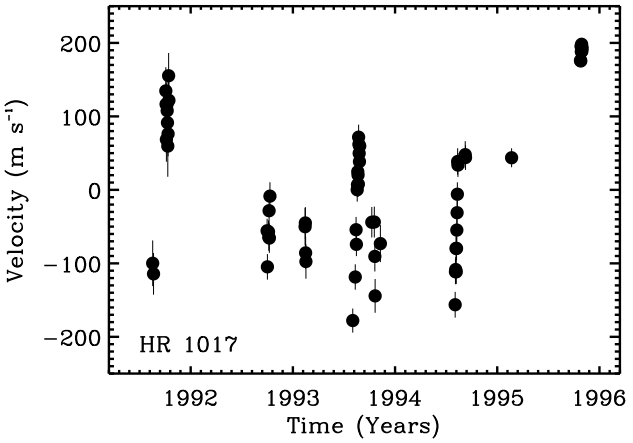

FIG. 11.—Measured Doppler velocities for HR 1017. A total of 63 observations span 4.2 yr. The rms of the velocities is 101 m s^{-1}, and the full amplitude of the velocity variation is $\sim$350 m s^{-1}.

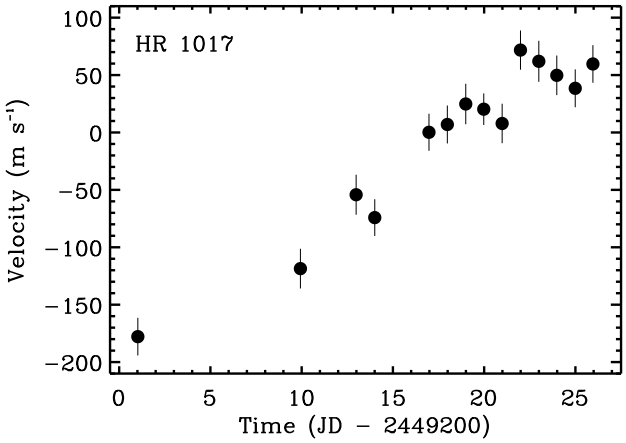

FIG. 13.—Fourteen measured Doppler velocities of HR 1017, spanning 25 nights in 1993 August. The velocities climb by more than 200 m s^{-1}.

with a period of 77.717 days in Figure 14. The solid line is a sinusoidal fit. The rms to the sinusoidal fit is 56.2 m s^{-1}. A periodogram of the residual velocities, after removing the sinusoidal fit, is shown in Figure 12*b*. Several peaks lie above the 1% false alarm level. These peaks may be real, or they may be an artifact of subtracting the overly simplistic sinusoid (Larson et al. 1993).

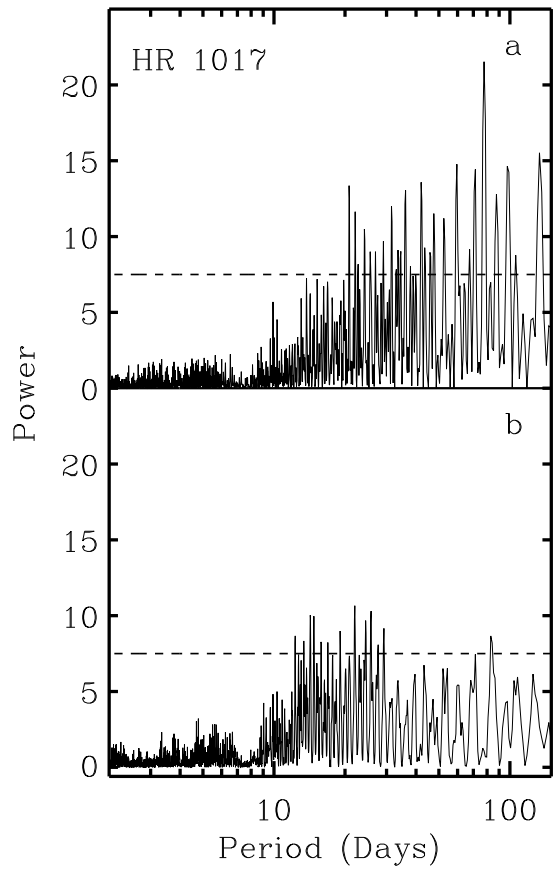

FIG. 12.—Periodogram of HR 1017 velocities. (*a*) Periodogram of measured velocities. The dominant peak has a period of 77.717 days. The 1% false alarm level is indicated by the dotted line. (*b*) Periodogram of residual velocities, after subtracting a best-fit sinusoid with a period of 77.717 days. The remaining periodogram peaks are significantly decreased, although several rise significantly above the 1% false alarm level.

3.6. *HR 1603 (G0Ib)*

The velocity measurements of HR 1603 are shown in Figure 15. Measurement uncertainty is $\sim$13 m s^{-1}, the rms of the measured velocities is 63.4 m s^{-1}, and the full amplitude of the velocity variations is $\sim$250 m s^{-1}. Velocities

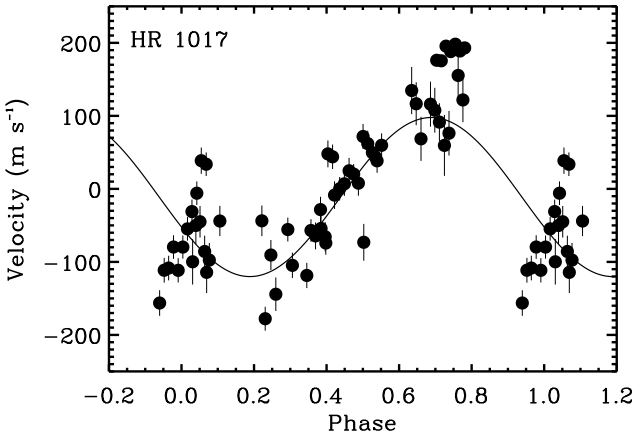

FIG. 14.—HR 1017 velocities phased with a 77.717 day period. The rms to the sinusoidal fit is 56 m s^{-1}.

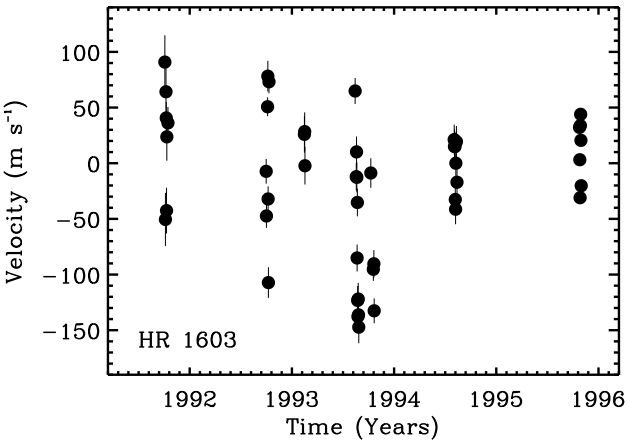

FIG. 15.—Measured Doppler velocities for HR 1603. The rms is 63 m s^{-1}, and the full amplitude of the velocity variation is $\sim$250 m s^{-1}.

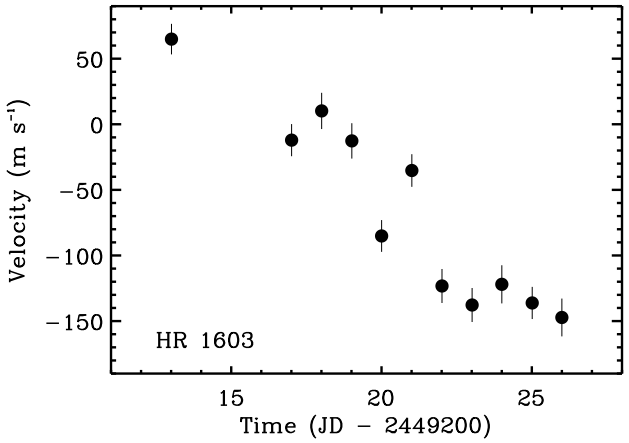

FIG. 16.—Eleven measured Doppler velocities of HR 1603, spanning 13 nights in 1993 August. The velocities descend by about 200 m s^{-1}.

spanning 13 nights (Fig. 16) show a clear downward trend of 200 m s^{-1}.

The periodogram of the velocities, shown in Figure 17*a*, reveals two peaks of almost equal strength at 44.717 and 51.575 days, with a third strong peak at 25.922 days. Sinusoids have been fitted to the data with the 44.717 and 51.575 day periods. The rms fit of the 44.717 day sine is 46.5 m s^{-1}, while that of the 51.575 day sine is 49.7 m s^{-1}. Figure 18*a* shows the velocities phased with the 44.717 day period, while Figure 18*b* shows the data phased with the 51.575 day period. Two sinusoidal models of the data have been created, with periods of 44.717 and 51.575 days, as in the case of HR 800. Random noise with a rms of 50 m s^{-1} was added to each of the sinusoids, and the sinusoids were then sampled at the same times as the observations. A total of 100 such models was constructed for each of the two periods, and periodograms were run for each case. The 44.717 day sinusoid produced strong peaks between 50.575 and 52.575 days 74% of the time, and between 24.9 and 26.9 days 30% of the time. For the case of the 51.575 sinusoid, strong peaks between 43.7 and 45.7 days were generated 62% of the time, and between 24.9 and 26.9 days 14% of the time. Both sets of models also typically produced periodogram peaks near 400 and 1000 days, as in Figure 17*a*. Thus, both a 44.717 and a 50.575 day period are consistent with the observed periodogram, although the 44.717 day period is more likely to produce the aliased peak near 26 days.

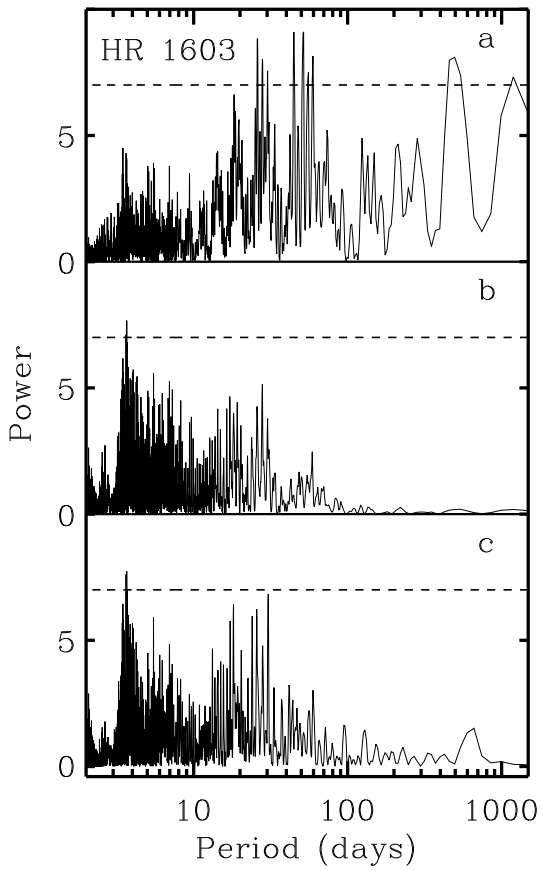

FIG. 17.—Periodogram of HR 1603 velocities. (*a*) Periodogram of measured velocities. The three highest periodogram peaks have periodicities of 44.717, 51.575, and 25.922 days. The 1% false alarm level is indicated by the dotted line. (*b*) Periodogram of residual velocities, after subtracting a best-fit sinusoid with a period of 44.717 days. Power at periods longer than 10 days is significantly reduced. (*c*) Periodogram of residual velocities, after subtracting a best-fit sinusoid with a period of 51.575 days. A few peaks near 20 and 30 days nearly rise to the 1% false alarm level.

A periodogram of the residual velocities, after removing a sinusoid with a 44.717 day period, is shown in Figure 17*b*. The periodogram of the residual velocities, after subtracting a sinusoid with a 51.575 day period, is shown in Figure 17*c*.

3.7. *HR 1884 (G3Ib)*

This star is listed as a possible spectroscopic binary by Burki & Mayor (1983). Figure 19 shows a total of 42 observations over 5.2 yr. There is a 4 × 10^4 m s^{-1} jump in velocities between the first and second observing runs. Subsequently, there is a monotonic 8 × 10^3 m s^{-1} decline in the velocities. The solid line in Figure 19 shows a possible orbital fit. The orbital period is 9390 days, and the rms of the orbital fit is 91 m s^{-1}. Only about a quarter of the proposed period has been sampled, so the orbit is quite tentative. It will not be possible to search other periodicities until the orbit has been more completely sampled.

3.8. *HR 6536 (G2Ib-IIa)*

The measured Doppler velocities of HR 6536 are shown in Figure 20. These velocities have a rms of 50.3 m s^{-1}. A periodogram of the Doppler velocities is shown in Figure

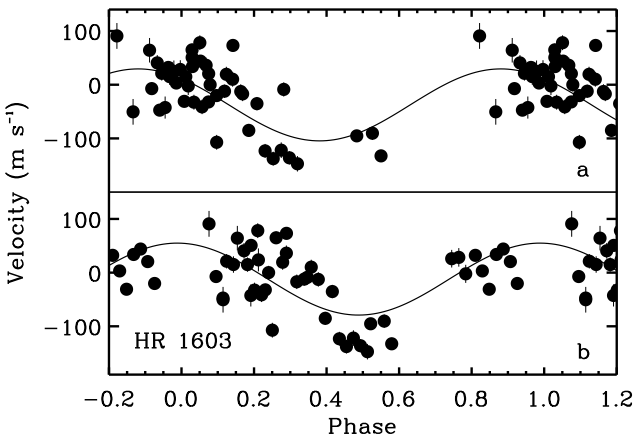

FIG. 18.—Phased Doppler velocities for HR 1603. (*a*) Doppler velocities phased with a 44.717 day period. The rms to the sinusoidal fit is 47 m s^{-1}. (*b*) Doppler velocities phased with a 51.575 day period. The rms to the sinusoidal fit is 50 m s^{-1}.

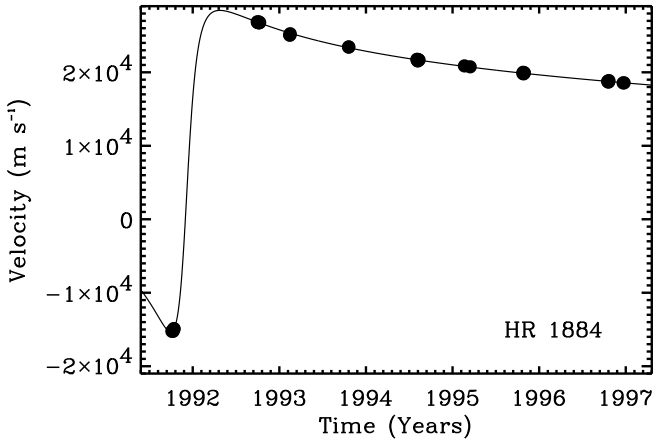

FIG. 19.—Measured Doppler velocities for HR 1884. A total of 42 observations span 5.2 yr. A possible Keplerian orbit is indicated by the line. The rms of the Keplerian fit is 90.7 m s^{-1}. The orbital period is ~26 yr, and the eccentricity is 0.89. Less than a quarter of the orbit has been observed, leaving the orbital parameters quite uncertain.

21*a*. The periods of the three highest peaks are 21.292, 20.073, and 108.065 days, respectively. Sinusoids fitted to the data with these periods scatter by 37.6, 38.8, and 38.2 m s^{-1}, respectively.

Figure 22 shows 13 observations of HR 6536 taken over 14 nights, beginning in 1993 mid-August. Over this 2 week interval the velocities change by the full amplitude of the variations in the entire data set, suggesting that the 108 day period is an alias of a shorter period.

One hundred sinusoidal models of the data have been constructed with each of the three peak periods from the periodogram. Random noise with a rms of 38 m s^{-1} has been added to the models, and periodograms have been taken of the results. Models constructed from 108.065 day sinusoid produced strong periodogram peaks between 17 and 24 days in 2% of the simulations. Models constructed from the 20.073 and the 21.295 day sinusoids produce strong peaks between 103 and 113 days for 1% and 13% of the time, respectively. Thus, it is likely that the 108 day periodicity seen in the periodogram is an alias of the 21.292 day period.

A periodogram of the residual velocities, after subtracting the sinusoidal fit at the 21.292 period, is shown in Figures 21*b*. A few peaks are seen above the 1% false alarm level

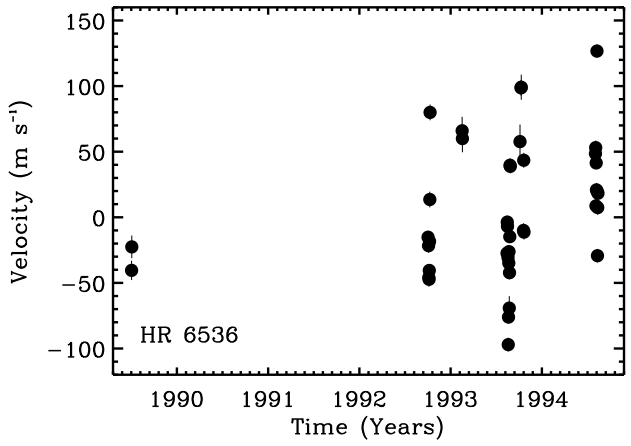

FIG. 20.—Measured Doppler velocities for HR 6536. The rms of the velocities is 50 m s^{-1}.

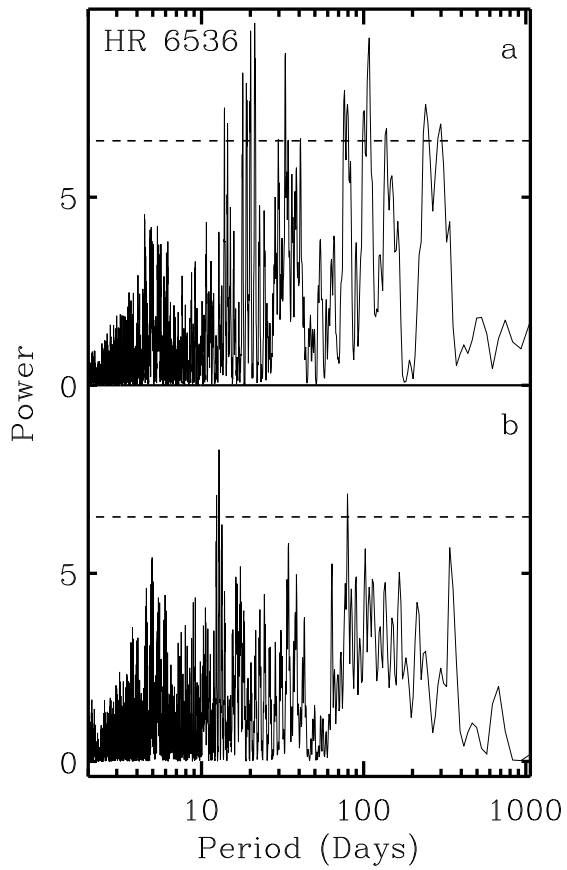

FIG. 21.—Periodogram of HR 6536 velocities. (*a*) Periodogram of measured velocities. The three highest peaks have periods of 21.292, 20.073, and 108.065 days. The 1% false alarm level is indicated by the dotted line. (*b*) Periodogram of residual velocities, after subtracting a best-fit sinusoid with a period of 21.292 days.

that are possibly artifacts of subtracting the overly simplistic sinusoid.

Figure 23*a* shows the velocities phased at the 21.292 day period, and Figure 23*b* shows the velocities phased with the 108.065 day period.

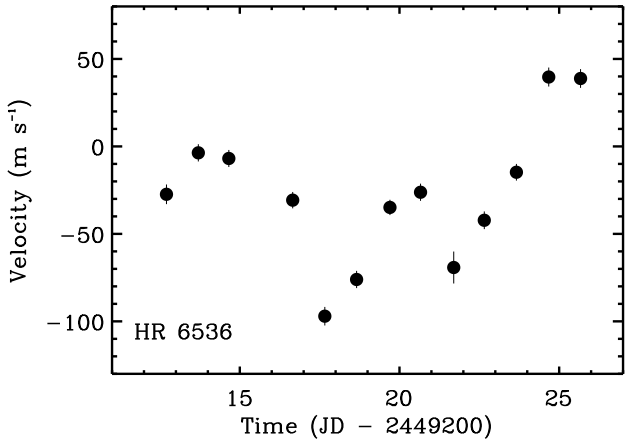

FIG. 22.—Thirteen measured Doppler velocities of HR 6536, spanning 14 nights in 1993 August. The amplitude of the velocity variations from this run are nearly as large as those from the entire data set.

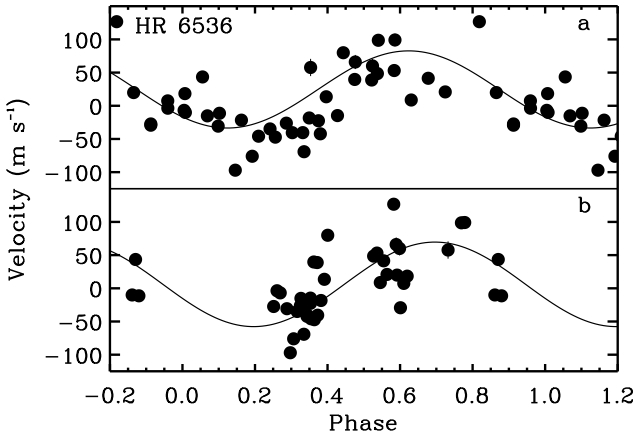

FIG. 23.—Phased Doppler velocities for HR 6536. (*a*) Doppler velocities phased with 21.292 day period. The rms to the sinusoidal fit is 37.6 m s^{-1}. (*b*) Doppler velocities phased with a 108.065 day period. The rms to the sinusoidal fit is 38.2 m s^{-1}.

3.9. *HR 6978 (F7Ib)*

The measured Doppler velocities of HR 6978 are shown in Figure 24. Meaurement uncertainty is $\sim$11 m s^{-1}, the rms of the velocities is 36 m s^{-1}, and the full amplitude of the velocity variation is $\sim$150 m s^{-1}. A periodogram of the Doppler velocities is shown in Figure 25*a*. The periods of the three highest peaks are 79.708, 65.000, and 157.690 days, respectively. Sinusoids fitted to the data at these periods have rms residuals of 27.4, 29.3, and 28.0 m s^{-1}, respectively.

A hundred sinusoidal models of the data have been constructed at each of the three peak periods. Random noise with a rms of 28 m s^{-1} has been added to the models, and periodograms have been determined for the results. The 79.708 day sinusoid produced strong periodogram peaks between 152.7 and 162.7 days 60% of the time, and between 64 and 66 days 59% of the time. The 65.000 day sinusoid produced peaks between 152.7 and 162.7 days 10% of the time, and between 78.5 and 81 days 29% of the time. The 157.690 day sinusoid produced peaks between 64 and 66 days 13% of the time, and between 78.5 and 81 days 26% of the time. Thus it is likely that both the 65 and the 157 day periodicities are aliases of the 79.708 day period. A periodogram of the velocity residuals, after removing the 79.708 day sinusoid, is shown in Figure 25*b*. There are no significant remaining peaks at the 1% false alarm level. Figure 26 shows the observed velocities, phased with the period of 79.708 days.

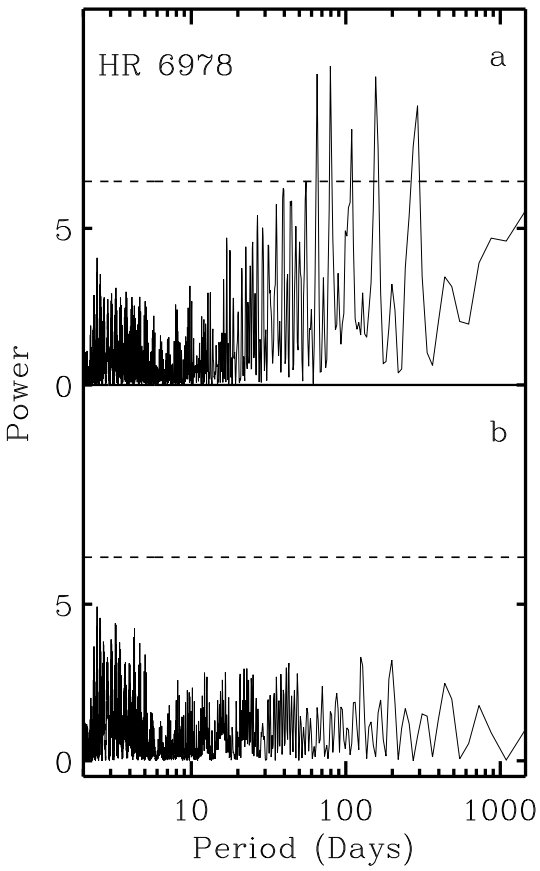

FIG. 25.—Periodogram of HR 6978 velocities. (*a*) Periodogram of measured velocities. The three highest peaks have periods of 79.708, 65.000, and 157.690 days. The 1% false alarm level is indicated by the dotted line. (*b*) Periodogram of residual velocities, after subtracting a best-fit sinusoid with a period of 79.708 days.

3.10. *HR 7387 (F2Ib)*

The measured Doppler velocities of HR 7387 are shown in Figure 27. This is the earliest spectral type of the program stars. As a result, the spectral lines are broader and less than

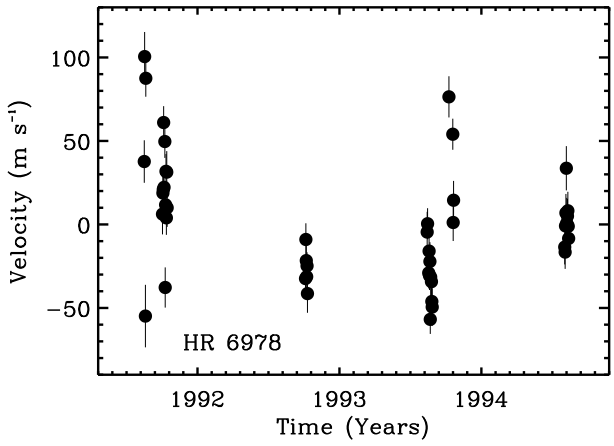

FIG. 24.—Measured Doppler velocities for HR 6978. A total of 48 observations span 3.0 yr. The rms of the velocities is 36 m s^{-1}.

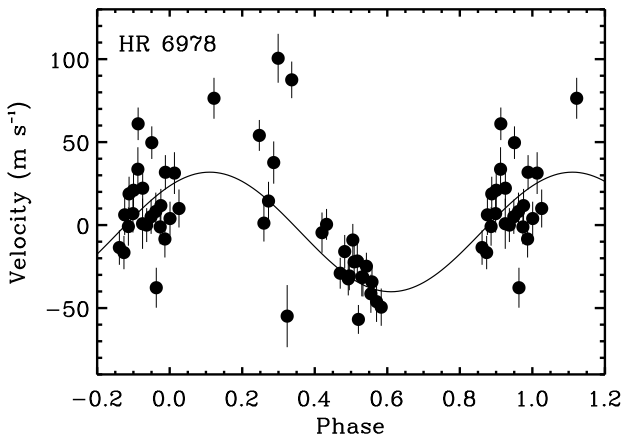

FIG. 26.—HR 6978 Doppler velocities phased with a period of 79.708 days. The rms to the sinusoidal fit is 27.4 m s^{-1}.

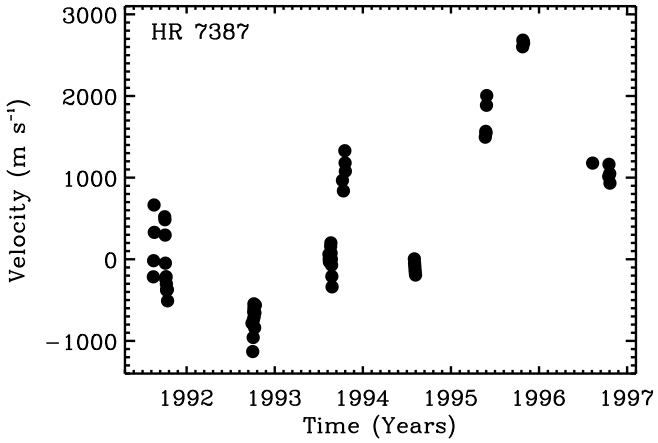

FIG. 27.—Measured Doppler velocities for HR 7387. A total of 64 observations span 5.2 yr. The rms is 950 m s^{-1}, and the full amplitude of the velocity variation is $\sim$3800 m s^{-1}.

one-half the depth of the typical star in this program. The uncertainty of the individual observations, $\sim$55 m s^{-1}, is more than 3 times greater than that of any other star in this program. Measurement uncertainty is nonetheless quite small, when compared to the intrinsic variability of the Doppler velocity signal. The rms of the measured velocities, 947.9 m s^{-1}, is so large that it suggests possible orbital motion.

The periodogram of the velocities is shown in Figure 28*a*. The periods of the highest peaks in the periodogram are 84.126, 39.352, and 173.257 days. Keplerian orbital fits to the data at periods of around 84 and 173 days yield rms residuals to the data of 321 and 508 m s^{-1}, respectively. Such large deviations do not strongly support the orbital hypothesis. Furthermore, orbits of 84 and 170 days would have semimajor axes of 0.65 and 1.03 AU, respectively, assuming a 5 $M_\odot$ primary. These orbits would be uncomfortably close to a star of $\sim$100 $R_\odot$. Figure 29 shows a sinusoidal fit (*solid line*) and a Keplerian fit (*dashed line*) to the velocities when phased at the 84.126 day period.

Sinusoids fitted to the data at the periods of the three highest periodogram peaks have rms residuals of 544, 687, and 601 m s^{-1}, respectively. One hundred sinusoidal models of the data have been constructed at each of the three peak periods. Random noise with a rms of 600 m s^{-1} has been added to the models, and periodograms have been determined for the results. The 84.126 day sinusoid produced strong periodogram peaks between 38.5 and 40.0 days 93% of the time, and between 163 and 183 days 61% of the time. The 39.352 day sinusoid produced peaks between 83.5 and 85.5 days 41% of the time, and between 163 and 183 days 23% of the time. The 173.257 day periodicity produced peaks between 83.5 and 85.5 days 66% of the time, and between 38.5 and 40.0 days 55% of the time. The 84 day periodicity is slightly more likely to produce aliased peaks that are similar to the observed periodogram, but neither the 173 nor the 39 day periods can be ruled out.

HR 7387 was repeatedly observed for more than 10 nights on three different observing runs. The results are shown in Figure 30. The velocity zero point of each of the observing runs is arbitrary. The circles are from an observing run that began in 1991 early October, and they span 12 nights; the squares are from 1992 late September and span 12 nights; and the diamonds are from 1993 mid-August and

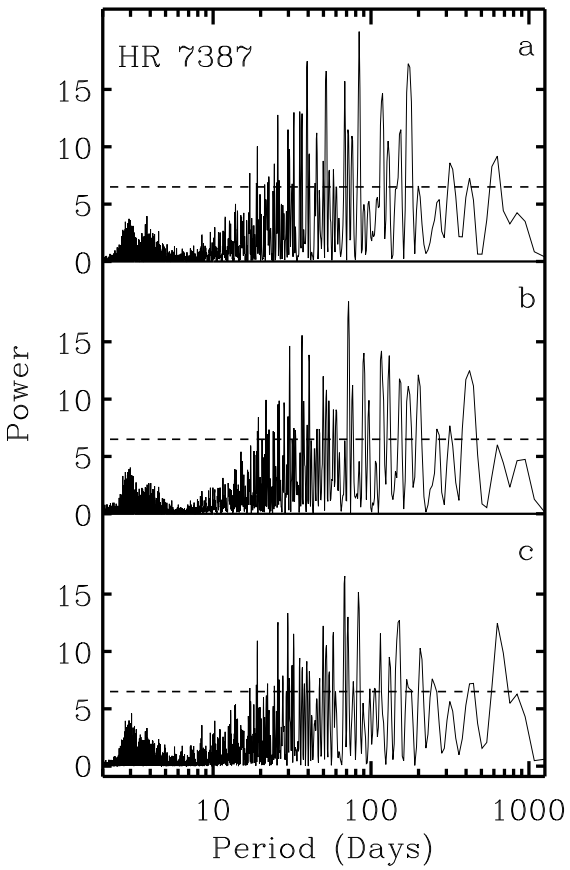

FIG. 28.—Periodogram of HR 7387 velocities. (*a*) Periodogram of measured velocities. The three highest periodogram peaks have periodicities of 84.126, 39.352, and 173.257 days. The 1% false alarm level is indicated by the dotted line. (*b*) Periodogram of residual velocities, after subtracting a best-fit sinusoid with a period of 84.126 days. (*c*) Periodogram of residual velocities, after subtracting a best-fit sinusoid with a period of 173.257 days.

span 13 nights. The night-to-night velocity variations are clearly correlated, with changes in velocity of $\sim$500 m s^{-1} occurring over $\sim$5 days. Given that the full amplitude of the observed velocity variation is $\sim$3000 m s^{-1}, this suggests that the longer 173 day peak from the periodogram is an alias.

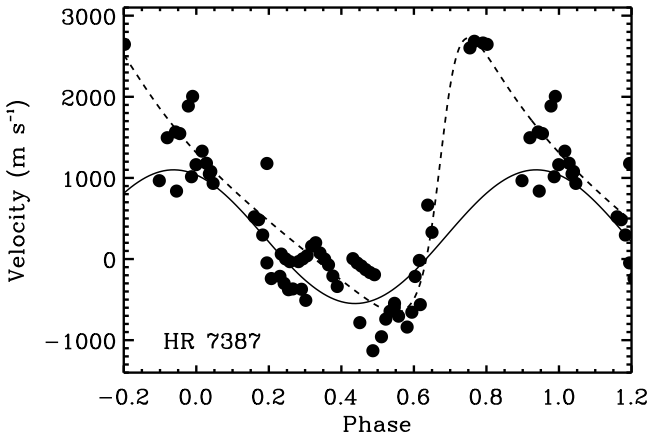

FIG. 29.—HR 7387 Doppler velocities phased with an 84.126 day period. The solid line is a sinusoidal fit, and the dashed line is a Keplerian fit. The rms to the sinusoidal fit is 544 m s^{-1}, while the rms of the Keplerian fit is 321 m s^{-1}.

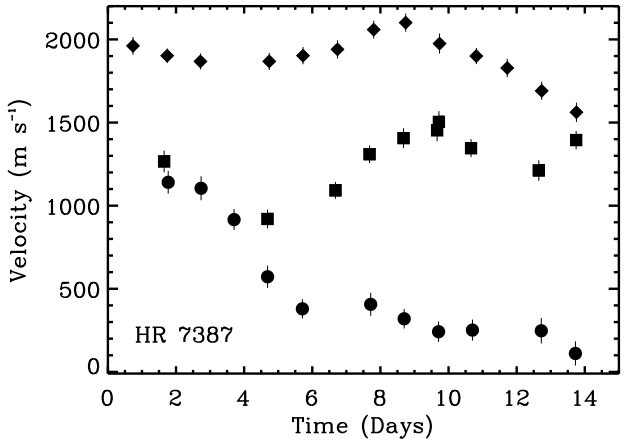

FIG. 30.—Nightly velocity variations of HR 7387 from three observing runs. The velocity zero point of each of these runs is arbitrary. *Circles:* Observing run that began in 1991 early October; *squares:* observing run that began in 1992 late September; *diamonds:* observing run that began in 1993 August. Velocity variations within a single run are typically ~ 500 m s^{-1}.

Velocity residuals to sinusoidal fits yield many periodogram peaks that are well above the 1% false alarm level. Figures 28*b* and 29*c* show the periodograms of the residual velocities to sinusoidal fits at the 84.126 and 173.257 day periods. The proliferation of strong periodogram peaks suggests that the star may have multiple periodicities.

3.11. *HR 7796 (F8Ib)*

The measured Doppler velocities for HR 7796 are shown in Figure 31. Butler (1992) previously reported that this star has a 11.9 day period and a 400 m s^{-1} full amplitude. This amplitude is clearly inconsistent with the 2×10^3 m s^{-1} variation seen in Figure 31. The periodogram of the velocities is shown in Figure 32*a*. All of the 10 highest peaks in the periodogram correspond to periodicities of more than 30 days.

The results of Butler (1992) were based on three observing runs. As that paper noted, "Each of the three observing runs had a different primary goal. For this reason the position of the CCD chip was somewhat different during each run. This has necessitated the use of a separate template spectrum for each of the program stars for each of the three runs." The effect of using a separate template spectrum for each run was to introduce an arbitrary velocity zero point for each of the three runs. These arbitrary velocity zero points disguised the large amplitude of the velocity variations and introduced the 11.9 day peak in the periodogram.

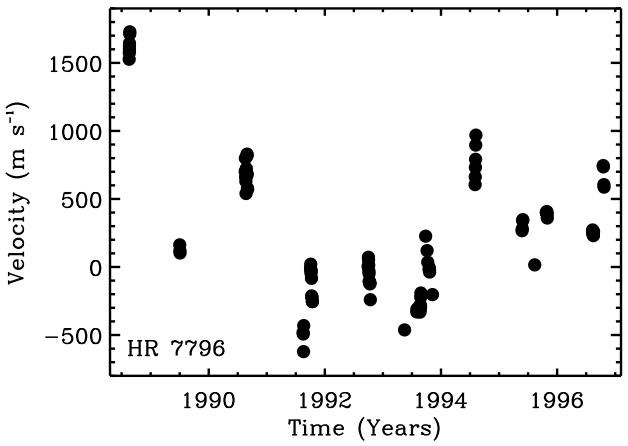

FIG. 31.—Measured Doppler velocities for HR 7796. A total of 105 observations span 8.2 yr. The rms is 537 m s^{-1}, and the full amplitude of the velocity variation is ~ 2200 m s^{-1}.

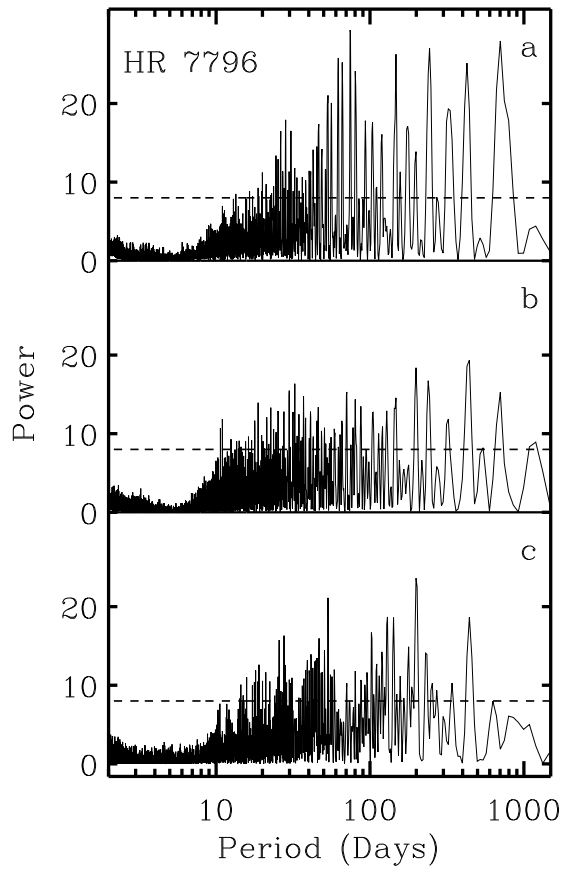

FIG. 32.—Periodogram of HR 7796 velocities. (*a*) Periodogram of measured velocities. The three highest periodogram peaks have periodicities of 74.440, 702.801, and 243.829 days. The 1% false alarm level is indicated by the dotted line. (*b*) Periodogram of residual velocities, after subtracting a best-fit sinusoid with a period of 74.440 days. (*c*) Periodogram of residual velocities, after subtracting a best-fit sinusoid with a period of 243.829 days.

All spectra prior to 1994 November were taken with an 800 × 800 CCD. Since then, a 2048 × 2048 CCD has been used exclusively. This larger format CCD covers the entire spectral range of all three observing runs reported in the 1992 paper. The same iodine absorption cell has been used to provide a velocity metric for all observations reported in this paper and in the 1992 paper. All of the data reported in the 1992 paper have been reanalyzed with a single new template taken with the 2048 × 2048 CCD. Since all observations have now been analyzed with the same stellar template spectrum, the problem of arbitrary run-to-run velocity zero points has been resolved.

The three highest periodogram peaks shown in Figure 32*a* correspond to periodicities of 74.440, 702.801, and 243.829 days. Sinusoids fitted to the data with these periods yield rms fits of 353, 403, and 374 m s^{-1}, respectively. One hundred sinusoidal models of the data have been constructed at each of the three peak periods. Random noise with a rms of 400 m s^{-1} has been added to the models, and periodograms have been determined for the results. The

74.440 day sinusoid produced strong periodogram peaks between 695 and 710 days 4% of the time, and between 241.4 and 246.2 days 8% of the time. The 702.801 day sinusoid produced no peaks between 241.4 and 246.2 days, and no peaks between 73.44 and 75.44 days. The 243.829 day periodicity produced peaks between 73.44 and 75.44 days 11% of the time, and between 695 and 710 days 7% of the time. Thus both 74.440 and 243.829 day periodicities yield aliases that consistent with the observed periodogram, but the 702.801 day periodicity does not.

HR 7796 was observed over a span of more than 10 nights on four occasions. The results are shown in Figure 33. The velocity zero point of each of the observing runs is arbitrary. The circles are from an observing run that began in 1990 mid-August, and span 14 nights. The squares are from 1991 early October, and span 12 nights. The diamonds are from 1992 late September and span 13 nights. The triangles begin in 1993 late July and span 25 nights. Velocity variations of 300 m s^{-1} are seen on timescales of 4 days to two weeks. Given the full amplitude of the observed velocity variation is $\sim$2000 m s^{-1}, this suggests that the longer period peaks from the periodogram are aliases.

In Figure 34*a* the measured velocities of HR 7796 are shown phased with the period of 74.440 days. While most observations fall within $\sim$100 m s^{-1} of the sine fit, observations from three observing runs sit 500 to 1000 m s^{-1} from the sine. A periodogram of the velocity residuals of HR 7796, after subtracting the 74.440 day sine fit, is shown in Figure 32*b*. In Figure 34*b* the velocities of HR 7796 are shown phased with the period of 243.829 days. A periodogram of the residual velocities, after subtracting the 243.829 day sine fit, is shown in Figure 32*c*. Many periodogram peaks in Figures 32*a* and 32*b* rise above the 1% false alarm level, suggesting the possibility of multiple periods.

3.12. *HR 7834 (F5II)*

The measured Doppler velocities of HR 7834 are shown in Figure 35. Though these velocities have an rms of only 23.8 m s^{-1}, the periodogram (Fig. 36*a*) shows several strong peaks above the 1% false alarm level. The strongest peak has a period of 70.674 days. Figure 37 shows the data

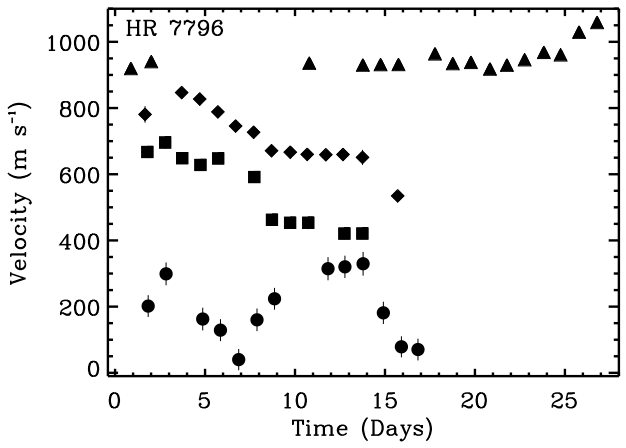

FIG. 33.—Nightly velocity variations of HR 7796 from four observing runs. The velocity zero point of each of these runs is arbitrary. *Circles:* Observing run that began in 1990 mid-August; *squares:* observing run that began in 1991 early October; *diamonds:* observing run that began in 1992 late September; *triangles:* observing run that began in 1993 late July. Velocity variations within a single run are typically $\sim$300 m s^{-1}.

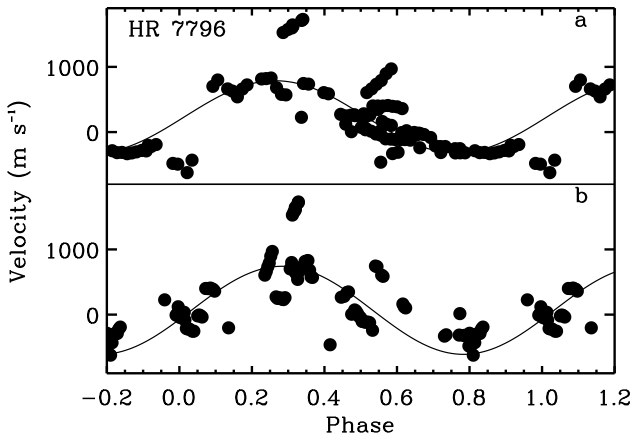

FIG. 34.—Phased Doppler velocities for HR 7796. (*a*) Doppler velocities phased with 74.440 day period. The rms to the sinusoidal fit is 353 m s^{-1}. (*b*) Doppler velocities phased with a 243.829 day period. The rms to the sinusoidal fit is 374 m s^{-1}.

phased with this period. The rms of the sine fit to this data is 17.6 m s^{-1}, which is only slightly larger than the internal measurement error of 12.5 m s^{-1}. The periodogram of the velocity residuals, after removing the 70.674 day sine fit, is shown in Figure 36*b*. There are no remaining periodogram peaks above the 1% false alarm level.

3.13. *HR 8232 (G0Ib)*

Doppler velocity measurements for HR 8232 are shown in Figure 38. Seventy observations span 4.2 yr and, the full

TABLE 4

HR 157 MEASURED DOPPLER VELOCITIES

MJD[a]	Velocity (m s^{-1})	Error (m s^{-1})
48894.846	10	12
48895.857	43	14
48897.848	−38	13
48899.835	−35	12
48900.828	−19	13
48901.888	12	11
48902.819	80	11
48903.827	30	11
48904.870	15	12
49030.631	45	20
49199.942	−27	5
49212.924	50	12
49217.931	−43	10
49218.921	−24	11
49220.934	22	11
49221.913	59	11
49223.905	−20	11
49225.916	35	11
49268.893	45	12
49277.893	0	15
49278.892	−35	14
49279.842	−18	14
49280.888	−7	11
49566.911	−12	10
49567.880	−28	11
49569.852	16	9
49570.864	−5	11
49571.902	22	10
49572.874	−3	10
49573.839	50	9
49575.836	45	12
49576.868	23	10

[a] Modified Julian Date = JD − 2,400,000.

TABLE 5

HR 213 Measured Doppler Velocities

MJD	Velocity (m s^{-1})	Error (m s^{-1})
48894.872.....	219	10
48895.881.....	242	10
48897.875.....	323	10
48899.860.....	363	8
48900.852.....	366	9
48901.911.....	440	9
48902.844.....	428	10
48903.882.....	452	8
48904.893.....	486	11
49268.917.....	−1238	10
49277.918.....	−1364	13
49278.914.....	−1318	12
49279.864.....	−1377	10
49280.911.....	−1450	10
49568.864.....	−9222	10
49569.899.....	−9219	12
49570.887.....	−9259	11
49573.862.....	−9238	12
49575.857.....	−9119	10
49576.890.....	−9096	10
49970.908.....	670	3
50012.784.....	225	4
50015.782.....	209	5
50016.796.....	228	5
50017.815.....	221	5
50018.801.....	202	5
50019.769.....	165	5
50020.776.....	151	5
50033.771.....	−4	4
50372.934.....	−8636	8
50373.805.....	−8660	6
50374.861.....	−8712	5
50376.833.....	−8763	7
50377.788.....	−8786	5
50437.735.....	−8432	7
50441.731.....	−8197	8

range of velocity variation is ~500 m s^{-1}. Murdoch et al. (1993) found a similar level of velocity variability, based on 29 observations taken over 2.7 yr. They report a periodicity in their velocities of 10^3 days or longer, which they attribute to orbital motion.

A periodogram of the velocities from Figure 38 is shown in Figure 39*a*. Two nearly equal peaks are seen at periods of 1023.866 and 203.417 days. Sinusoidal fits to the velocities

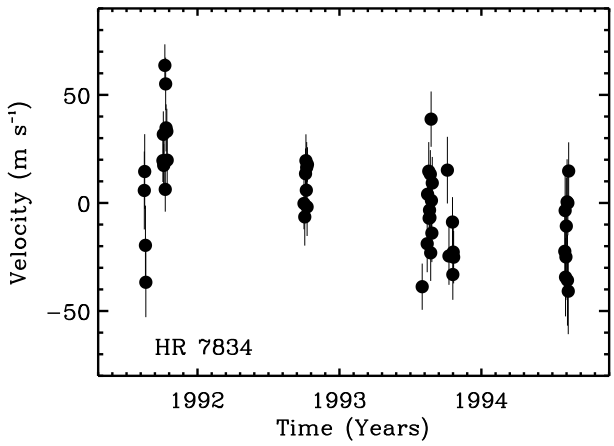

Fig. 35.—Measured Doppler velocities for HR 7834. A total of 51 observations span 3.0 yr. The rms is 24 m s^{-1}, and the full amplitude of the velocity variation is ~100 m s^{-1}.

TABLE 6

HR 461 Measured Doppler Velocities

MJD	Velocity (m s^{-1})	Error (m s^{-1})
48894.897.....	141	13
48895.905.....	37	9
48897.898.....	78	9
48899.883.....	68	9
48900.874.....	110	10
48901.935.....	139	12
48902.867.....	104	9
48903.905.....	139	9
48904.945.....	75	10
49030.656.....	166	18
49213.935.....	−74	10
49218.944.....	−124	12
49221.936.....	−127	12
49223.927.....	0	12
49224.938.....	−6	11
49268.941.....	−112	10
49277.951.....	−115	11
49278.936.....	−58	11
49279.887.....	−108	9
49280.933.....	−122	12
49567.927.....	−11	11
49569.876.....	−12	10
49570.909.....	−112	11
49572.897.....	−93	9
49574.900.....	−44	9
49576.920.....	35	11
50015.805.....	51	5
50017.884.....	−1	5
50018.823.....	14	5
50019.792.....	61	5
50020.798.....	96	6

at these two periods have a rms of 100.2 and 98.8 m s^{-1}, respectively. One hundred sinusoidal models of the data at these periods have been constructed. Random noise with a rms of 100 m s^{-1} has been added to the models, and periodograms have been determined for the results. The 1023 day sinusoid produced strong periodogram peaks between 200 and 207 days 66% of the time. The 203 day sinusoid produced peaks between 1005 and 1042 days 42% of the time. Thus, both the 1023 and 203 day periodicities yield aliases that are consistent with the observed periodogram.

HR 8232 was observed over a span of 10 or more nights on three occasions, as shown in Figure 40. The velocity zero point of each of the observing runs is arbitrary. The circles are from an observing run that began in 1991 early October and span 11 nights, the squares are from 1993 early August and span 25 nights, and the diamonds are from 1994 early August and span 10 nights. Velocity variations of ~100 m s^{-1} are seen on timescales of 1–5 days. Given that the full amplitude of the observed velocity variation is ~500 m s^{-1}, this suggests that the 1023 day period is the alias of the shorter 203 day period. In Figure 41*a* the velocities are shown phased with the 1023.866 day period, while in Figure 41*b* they are phased with the 203.417 day period.

Periodograms of the residual velocities, after removing the best-fit sinusoid at the 1023 and 203 day periods, are shown in Figures 38*b* and 38*c*, respectively. A number of peaks rise above the 1% false alarm level after removing the 1023 day periodicity, while no such peaks are seen after removing the 203 day period.

3.14. *HR 8313 (G5Ib)*

The measured Doppler velocities of HR 8313 are shown

TABLE 7

HR 800 Measured Doppler Velocities

MJD	Velocity (m s^{-1})	Error (m s^{-1})
48485.003.....	25	23
48485.994.....	110	23
48487.958.....	209	26
48488.993.....	157	21
48532.908.....	−27	24
48533.875.....	−19	25
48534.880.....	14	24
48536.932.....	147	36
48537.862.....	69	22
48538.846.....	63	24
48539.868.....	29	23
48540.887.....	−19	24
48542.866.....	21	25
48543.876.....	14	15
48894.962.....	50	18
48895.943.....	−32	18
48897.936.....	61	30
48899.923.....	−7	16
48900.909.....	92	16
48901.972.....	42	18
48902.914.....	−29	12
48903.970.....	−43	17
48904.980.....	6	16
49030.681.....	−2	19
49032.626.....	68	18
49033.626.....	45	20
49212.949.....	−110	16
49213.975.....	−73	18
49214.936.....	28	13
49216.944.....	−138	16
49217.953.....	−119	16
49218.966.....	−86	22
49219.947.....	−37	17
49220.956.....	−91	14
49221.960.....	−80	17
49222.968.....	−81	16
49223.950.....	−126	16
49224.962.....	−143	15
49225.939.....	−88	21
49264.885.....	−188	27
49268.987.....	−62	19
49277.992.....	−38	19
49278.970.....	−124	19
49279.923.....	−71	17
49280.976.....	−57	19
49566.955.....	−78	16
49567.904.....	−7	17
49568.887.....	−44	20
49569.922.....	25	18
49570.932.....	0	18
49571.926.....	24	15
49572.920.....	33	16
49573.884.....	−56	15
49574.923.....	14	13
50014.956.....	44	9
50015.934.....	85	7
50016.899.....	59	9
50017.930.....	19	7
50018.916.....	37	9
50019.884.....	48	7
50020.888.....	125	8

TABLE 8

HR 1017 Measured Doppler Velocities

MJD	Velocity (m s^{-1})	Error (m s^{-1})
48486.011.....	−100	31
48489.011.....	−114	28
48532.950.....	135	32
48533.919.....	117	29
48534.945.....	69	30
48536.977.....	116	31
48537.903.....	108	31
48538.886.....	91	26
48539.965.....	60	42
48540.942.....	76	31
48542.906.....	155	31
48543.927.....	122	31
48894.999.....	−56	16
48895.975.....	−105	17
48899.959.....	−57	15
48900.937.....	−64	18
48901.999.....	−28	18
48902.999.....	−66	20
48905.008.....	−9	19
49030.721.....	−50	26
49031.618.....	−45	22
49032.609.....	−86	22
49033.610.....	−97	23
49201.022.....	−178	16
49209.932.....	−119	17
49212.985.....	−54	17
49214.005.....	−74	16
49216.975.....	0	16
49217.982.....	7	17
49218.991.....	25	18
49219.977.....	20	14
49220.985.....	8	17
49221.989.....	72	17
49222.995.....	62	18
49223.980.....	50	17
49224.991.....	38	16
49225.959.....	60	16
49269.018.....	−44	21
49278.023.....	−44	21
49279.953.....	−91	21
49281.011.....	−144	23
49299.855.....	−73	25
49566.982.....	−156	18
49567.966.....	−111	17
49568.910.....	−108	17
49569.953.....	−80	16
49570.955.....	−112	17
49571.960.....	−80	16
49572.947.....	−55	16
49573.911.....	−31	17
49574.949.....	−6	16
49575.905.....	39	18
49576.964.....	34	16
49603.039.....	48	18
49604.039.....	44	17
49768.652.....	44	13
50014.939.....	176	6
50015.918.....	175	6
50016.938.....	195	6
50017.946.....	188	7
50018.933.....	198	7
50019.923.....	189	7
50020.928.....	193	6

in Figure 42. The rms of the observed velocities is 84 m s^{-1}, while the full range of velocity variation is $\sim$400 m s^{-1}. The velocity variation within individual observing runs is 100–300 m s^{-1}.

The three highest peaks in the velocity periodogram, shown in Figure 43*a*, have periods of 230.918, 137.823, and 711.549 days, respectively. Sinusoids fitted to the data with these periods yield rms fits of 63, 62, and 68 m s^{-1}, respectively. One hundred sinusoidal models of the data have been constructed at each of the three peak periods. Random noise with an rms of 63 m s^{-1} has been added to the models, and periodograms have been determined for the

TABLE 9

HR 1603 Measured Doppler Velocities

MJD	Velocity (m s^{-1})	Error (m s^{-1})
48532.986.....	91	24
48534.981.....	−51	24
48537.013.....	64	23
48537.964.....	41	15
48538.934.....	−43	21
48540.011.....	24	21
48543.986.....	36	14
48895.018.....	−7	11
48896.004.....	−47	11
48900.000.....	51	8
48900.949.....	78	14
48902.021.....	−32	11
48903.023.....	−107	14
48905.029.....	73	10
49031.677.....	26	16
49032.689.....	28	17
49033.672.....	−2	17
49213.012.....	65	12
49217.008.....	−12	12
49218.008.....	10	14
49219.012.....	−13	13
49220.003.....	−85	12
49221.008.....	−35	12
49222.012.....	−123	13
49223.013.....	−138	13
49224.002.....	−122	15
49225.013.....	−136	12
49225.999.....	−147	14
49269.029.....	−9	13
49278.033.....	−95	10
49279.964.....	−90	12
49281.024.....	−133	11
49567.005.....	21	13
49567.975.....	15	15
49569.972.....	15	13
49570.974.....	−33	14
49571.978.....	−41	13
49572.973.....	0	13
49574.973.....	19	14
49576.978.....	−17	13
50014.981.....	32	6
50015.974.....	3	5
50016.954.....	−31	5
50017.966.....	34	5
50018.950.....	44	5
50019.963.....	21	5
50020.945.....	−20	5

TABLE 10

HR 1884 Measured Doppler Velocities

MJD	Velocity (m s^{-1})	Error (m s^{-1})
48535.019.....	−35252	20
48537.038.....	−35141	26
48538.035.....	−35137	28
48538.981.....	−35205	24
48540.034.....	−35239	26
48543.031.....	−34875	20
48544.032.....	−34923	18
48895.044.....	6871	15
48896.025.....	6778	20
48900.048.....	6752	17
48900.994.....	6869	12
48902.039.....	6763	17
48903.042.....	6741	16
48905.046.....	6775	13
49031.704.....	5066	18
49032.712.....	5070	22
49033.698.....	5250	17
49279.996.....	3439	10
49281.046.....	3446	17
49567.995.....	1741	19
49569.999.....	1768	15
49570.992.....	1578	17
49571.997.....	1556	15
49572.991.....	1697	17
49574.990.....	1688	13
49576.994.....	1673	16
49768.670.....	872	13
49792.677.....	749	14
50015.005.....	−156	10
50015.997.....	0	10
50016.976.....	−84	13
50017.988.....	−210	10
50018.972.....	−129	13
50019.986.....	−57	11
50020.967.....	−73	10
50372.980.....	−1227	14
50373.926.....	−1222	10
50374.953.....	−1323	10
50376.934.....	−1300	11
50377.901.....	−1126	12
50437.890.....	−1438	11
50441.857.....	−1437	11

results. The 230.918 day sinusoid produced strong periodogram peaks between 136 and 140 days 44% of the time, and between 703 and 720 days 26% of the time. The 137.823 day sinusoid produced strong peaks between 227 and 235 days 67% of the time, and between 703 and 720 days 12% of the time. The 711.549 day periodicity produced peaks between 227 and 235 days 27% of the time, and between 136 and 140 days 6% of the time. Thus, all three periodicities produce aliases that can account for the observed periodogram.

HR 8313 was observed over a span of 10 or more nights on three occasions, as shown in Figure 44. The velocity zero point of each of the observing runs is arbitrary. The circles are from an observing run that began in 1991 early October, spanning 11 nights; the squares are from 1993 late July, spanning 25 nights; the diamonds are from 1993 early October, spanning 11 nights. Velocity variations of $\sim$200 m s^{-1} are seen on timescales of a few days. The full amplitude of the observed velocity variation is $\sim$400 m s^{-1}, which argues against the longer periods.

Periodograms of the residual velocities, after removing the best-fit sinusoid at the 230.918 and 137.822 day periods, are shown in Figures 38*b* and 38*c*, respectively. There are no remaining strong peaks in either periodogram.

3.15. *HR 8414 (G2Ib)*

The measured velocities of HR 8414 are shown in Figure 45. The rms is 122.8 m s^{-1}, and the full range of the velocity variations is $\sim$500 m s^{-1}.

A periodogram of the velocities is shown in Figure 46*a*. The three highest peaks have corresponding periods of 76.152, 40.626, and 121.987 days, respectively. Sinusoids fitted to the data with these periods yield rms fits of 87, 93, and 95 m s^{-1}, respectively. One hundred sinusoidal models of the data have been constructed at each of the three peak periods. Random noise with a rms of 90 m s^{-1} has been added to the models, and periodograms have been determined for the results. The 76.152 day sinusoid produced no strong periodogram peaks between 38 and 43 days and none between 110 and 132 days. It did produce strong

TABLE 11

HR 6536 MEASURED DOPPLER VELOCITIES

MJD	Velocity (m s^{-1})	Error (m s^{-1})
47709.855.....	−40	7
47710.772.....	−23	9
48896.636.....	−15	5
48898.634.....	−22	5
48899.641.....	−46	7
48900.626.....	−47	5
48901.621.....	−41	5
48902.616.....	−18	5
48903.613.....	14	6
48904.615.....	80	6
49033.074.....	66	11
49034.085.....	60	10
49212.704.....	−27	6
49213.702.....	−4	5
49214.657.....	−7	5
49216.657.....	−31	5
49217.662.....	−97	5
49218.657.....	−76	5
49219.702.....	−35	4
49220.659.....	−26	5
49221.699.....	−69	9
49222.655.....	−42	5
49223.662.....	−15	5
49224.674.....	40	5
49225.670.....	39	5
49264.669.....	58	13
49268.645.....	99	6
49269.621.....	99	10
49278.611.....	−10	5
49279.617.....	43	6
49280.611.....	−11	6
49566.685.....	49	5
49567.673.....	53	5
49568.672.....	9	5
49569.670.....	41	5
49570.669.....	21	5
49572.671.....	127	5
49573.668.....	20	6
49574.675.....	−29	5
49575.669.....	7	6
49576.679.....	18	5

TABLE 12

HR 6978 MEASURED DOPPLER VELOCITIES

MJD	Velocity (m s^{-1})	Error (m s^{-1})
48484.728.....	38	13
48485.704.....	101	15
48487.687.....	−55	19
48488.685.....	88	11
48531.687.....	6	12
48532.647.....	19	10
48533.627.....	21	12
48534.637.....	61	10
48535.636.....	22	11
48537.640.....	50	10
48538.626.....	−38	12
48539.634.....	12	10
48540.626.....	32	10
48541.643.....	4	10
48542.618.....	31	13
48543.619.....	10	11
48899.657.....	−32	10
48900.653.....	−9	10
48901.640.....	−22	10
48902.635.....	−31	12
48903.636.....	−25	8
48904.628.....	−41	11
49212.718.....	−5	12
49213.718.....	0	9
49216.719.....	−29	9
49217.704.....	−16	10
49218.718.....	−31	9
49219.781.....	−22	12
49220.720.....	−57	9
49221.713.....	−31	12
49223.700.....	−34	10
49224.706.....	−46	12
49225.731.....	−49	11
49268.689.....	76	12
49278.650.....	54	9
49279.656.....	1	11
49280.671.....	14	12
49566.728.....	−14	10
49567.733.....	−17	10
49568.709.....	−1	12
49569.706.....	7	11
49570.795.....	34	13
49571.824.....	1	15
49572.729.....	0	10
49573.702.....	5	10
49574.732.....	8	11
49575.703.....	−1	10
49576.736.....	−8	11

peaks between 95.4 and 96.8 days in 53% of the trials, which corresponds to the period (96.367 days) of the fourth highest periodogram peak in Figure 46*a*. The 40.626 day sinusoid produced strong peaks between 75 and 77 days 3% of the time and between 121 and 123 days 35% of the time. The 121.987 day periodicity produced no strong peaks between 70 and 80 days, but between 40 and 41 days, it produced a strong peak 39% of the time. It is not surprising that the 40.626 and 121.987 day periods generate "cross-aliases" so often, since the periods differ by almost exactly a factor of 3. Neither the 40.626 or 121.987 day periodicities produced aliases between 95 and 98 days.

HR 8414 was observed over a span of 10 or more nights on four occasions, as shown in Figure 47. The velocity zero point of each of the observing runs is arbitrary. The circles represent an observing run that began in 1990 mid-August, spanning 18 nights, the squares designate that of 1991 early October, spanning 12 nights, and the diamonds, late of 1992 late September, spanning 10 nights. The triangles represent 1993 mid-August and span 13 nights. Velocity variations of $\sim$150 m s^{-1} are seen in each of these observing runs. In Figure 48*a* the velocities are shown phased with the 76.152 day period, while in Figure 48*b* they are phased with the 40.626 day period.

The periodogram of the residual velocities, after removing the 76.152 day sinusoid, is shown in Figure 46*b*. A number of strong peaks are seen between about 80 and 235 days. A periodogram of the residuals, after removing the 40.626 day period, is shown in Figure 46*c*. The strong peaks in this periodogram are found at less than 100 days, with a cluster around 30 days.

4. LINE PROFILES

The colors and temperatures of nonvariable supergiants have been compared to Cepheids by several groups (Schmidt 1972; Evans 1993; Evans et al. 1993; Evans et al. 1996; Evans & Teays 1996; Bersier 1996). At their hottest phases, Cepheids have an enhanced flux at 3000 Å (Evans 1993), relative to the nonvariable supergiants. Further into the UV, near 1900 Å, the nonvariable supergiants have

TABLE 13

HR 7387 Measured Doppler Velocities

MJD	Velocity (m s^{-1})	Error (m s^{-1})
48484.805.....	−215	69
48485.788.....	−17	55
48487.736.....	665	64
48488.736.....	330	57
48531.771.....	521	68
48532.736.....	485	72
48533.704.....	296	63
48534.687.....	−48	67
48535.709.....	−240	58
48537.714.....	−214	69
48538.697.....	−300	58
48539.707.....	−378	61
48540.701.....	−368	63
48542.722.....	−373	76
48543.724.....	−509	73
48893.651.....	−784	66
48896.685.....	−1130	56
48898.681.....	−958	51
48899.681.....	−740	53
48900.678.....	−644	60
48901.664.....	−596	66
48901.717.....	−546	64
48902.660.....	−704	54
48904.649.....	−838	61
48905.745.....	−655	55
48907.712.....	−562	37
49212.737.....	61	54
49213.740.....	2	43
49214.717.....	−32	48
49216.737.....	−32	52
49217.728.....	2	52
49218.740.....	40	54
49219.803.....	159	54
49220.742.....	201	55
49221.735.....	75	60
49222.815.....	0	48
49223.722.....	−72	55
49224.734.....	−209	54
49225.754.....	−338	58
49268.717.....	966	58
49272.724.....	838	56
49278.673.....	1330	56
49279.678.....	1180	62
49280.693.....	1079	61
49566.752.....	5	52
49567.748.....	−49	56
49568.723.....	−86	62
49569.721.....	−130	55
49570.726.....	−166	58
49571.770.....	−193	58
49860.937.....	1495	20
49862.854.....	1567	20
49863.850.....	1547	20
49865.840.....	1886	19
49866.840.....	2005	21
50015.661.....	2603	17
50016.699.....	2684	18
50018.693.....	2663	20
50019.656.....	2646	31
50305.810.....	1178	22
50372.613.....	1015	20
50373.665.....	1163	19
50376.762.....	1049	22
50377.643.....	932	18

TABLE 14

HR 7796 Measured Doppler Velocities

MJD	Velocity (m s^{-1})	Error (m s^{-1})
47390.851.....	1527	7
47391.850.....	1574	11
47392.674.....	1598	18
47392.782.....	1644	19
47392.868.....	1621	19
47394.662.....	1712	20
47394.910.....	1728	21
47708.952.....	163	13
47709.874.....	120	12
47710.836.....	103	12
48120.839.....	702	33
48121.834.....	799	34
48123.871.....	663	34
48124.856.....	629	33
48125.870.....	540	32
48126.887.....	660	34
48127.862.....	724	33
48130.834.....	815	35
48131.774.....	820	34
48132.784.....	830	36
48133.910.....	681	34
48134.913.....	579	32
48135.833.....	570	33
48484.829.....	−481	17
48485.837.....	−492	16
48487.757.....	−622	23
48488.759.....	−431	16
48531.793.....	−8	18
48532.783.....	21	19
48533.730.....	−27	17
48534.744.....	−47	16
48535.730.....	−27	17
48537.736.....	−83	16
48538.720.....	−213	16
48539.727.....	−222	17
48540.734.....	−222	19
48542.744.....	−254	18
48543.743.....	−254	17
48893.665.....	6	25
48895.700.....	72	19
48896.704.....	52	20
48897.713.....	13	18
48898.699.....	−29	19
48899.699.....	−48	19
48900.695.....	−104	18
48901.735.....	−108	19
48902.677.....	−115	19
48903.714.....	−116	17
48904.667.....	−115	19
48905.751.....	−124	23
48907.707.....	−240	17
49123.012.....	−462	16
49199.879.....	−330	13
49201.010.....	−309	14
49209.792.....	−314	13
49212.772.....	−320	13
49213.756.....	−318	13
49214.750.....	−318	13
49216.779.....	−286	12
49217.771.....	−315	11
49218.777.....	−312	13
49219.836.....	−332	12
49220.777.....	−320	12
49221.762.....	−304	12
49222.830.....	−282	12
49223.761.....	−289	12
49224.788.....	−220	14
49225.790.....	−191	13
49255.615.....	226	27
49264.708.....	120	18

excess flux relative to the Cepheids and to static plane-parallel model atmospheres (Evans & Teays 1996). *ROSAT* observations indicate that the X-ray flux of Cepheids is at least a factor of 20 less than that of nonvariable supergiants

TABLE 14—*Continued*

MJD	Velocity (m s^{-1})	Error (m s^{-1})
49268.763.....	35	20
49277.810.....	−20	19
49278.765.....	−6	20
49279.721.....	−16	18
49280.766.....	−37	18
49298.598.....	−203	28
49566.789.....	605	23
49567.779.....	663	13
49568.758.....	732	12
49569.757.....	791	13
49570.755.....	896	16
49571.811.....	969	14
49861.995.....	267	6
49863.917.....	280	6
49865.892.....	341	6
49866.867.....	348	5
49941.738.....	15	7
50014.674.....	401	5
50015.685.....	400	4
50016.716.....	399	6
50017.767.....	407	5
50018.714.....	395	6
50019.675.....	387	6
50020.687.....	360	7
50305.828.....	272	5
50306.788.....	249	6
50307.872.....	258	8
50308.759.....	252	8
50309.851.....	236	8
50310.833.....	230	8
50311.824.....	260	8
50372.633.....	745	7
50373.682.....	736	9
50376.804.....	605	8
50377.758.....	587	8

(Sasselov & Sabbey 1994). In the visible and near-IR, Cepheids and nonvariable supergiants are photometrically quite similar.

The spectra of the three G0 supergiants in this sample are compared to δ Cep in Figure 49. The spectrum of δ Cep was taken from Butler (1993), and the phase (0.66) was choosen to match approximately the $B-V$ of the three G0 supergiants. The maximum infall velocity occurs at phase = 0.8, and 12 Å near Hβ is shown. The δ Cep Hβ line is somewhat narrower than that of the three G0 supergiants. The δ Cep Hα line at this phase is also similarly narrower. In all other respects, the spectra of the G0 supergiants are extremely similar to δ Cep, both in terms of line strengths and widths.

The five F supergiants in this sample are compared to δ Cep in Figure 50. The spectrum of δ Cep was again choosen to provide an approximate $B-V$ match to the F supergiants, which occurs near phase = 0.07. There is little to distinguish δ Cep from the later F stars in this group.

All the other program stars are redder than δ Cep, but they are spectroscopically similar to δ Cep at its reddest phases.

5. DISCUSSION

Fifteen F and G supergiants have been monitored for 4–8 yr. Doppler velocity measurement errors for these stars are typically less than 20 m s^{-1}, except for HR 7387, which is the earliest spectral type of any star in the program. The velocity scatter of every star is greater than the internal measurement error, although four stars (HR 157, HR 213, HR 6978, and HR 7834) are "stable" at the 30 m s^{-1} level. For comparison, slowly rotating late F and G main-sequence dwarfs are stable at the 3–5 m s^{-1} level (Butler et al. 1996; Butler & Marcy 1997).

TABLE 15

HR 7834 Measured Doppler Velocities

MJD	Velocity (m s^{-1})	Error (m s^{-1})
48484.871.....	6	18
48485.858.....	15	17
48487.779.....	−20	18
48488.783.....	−37	16
48532.760.....	20	10
48533.759.....	32	11
48534.769.....	17	10
48535.751.....	18	11
48537.757.....	64	10
48538.739.....	6	10
48539.747.....	55	12
48540.765.....	35	11
48542.768.....	33	10
48543.764.....	20	11
48895.721.....	0	12
48897.729.....	−6	13
48899.711.....	14	12
48900.708.....	20	12
48901.746.....	6	14
48902.689.....	16	12
48903.725.....	−2	13
48904.686.....	18	8
49199.887.....	−39	11
49212.782.....	−19	13
49213.792.....	4	11
49216.795.....	15	13
49217.793.....	−7	11
49218.788.....	−3	12
49219.848.....	−7	12
49220.789.....	13	11
49221.773.....	−23	13
49222.842.....	39	13
49223.773.....	1	13
49224.805.....	−14	13
49225.802.....	9	12
49264.716.....	15	15
49268.775.....	−25	13
49277.826.....	−9	12
49278.778.....	−33	12
49279.732.....	−23	14
49280.778.....	−25	12
49566.804.....	−22	17
49567.787.....	−4	19
49568.769.....	−34	18
49569.763.....	−25	20
49570.760.....	−11	22
49572.781.....	0	20
49573.750.....	−36	21
49574.785.....	0	15
49575.752.....	−41	20
49576.784.....	15	13

Periodograms of the Doppler velocities of most of the stars show multiple peaks. Nine of the 15 program stars have primary peaks with periodicities between 44 and 84 days, while two of the stars have primary peaks of ~200 days. There is no obvious correlation between periodicities and spectral type.

The variability in the measured Doppler velocities for the program stars is 1–3 orders of magnitude smaller than that of bona fide Cepheids, and the phased velocity curves are not reminiscent of Cepheid velocity curves.

With the exception of HR 213 and HR 1884, orbital

TABLE 16

HR 8232 Measured Doppler Velocities

MJD	Velocity (m s^{-1})	Error (m s^{-1})
48484.900.....	−80	14
48485.920.....	−43	14
48487.820.....	245	13
48488.804.....	−106	13
48531.851.....	−145	14
48532.802.....	−80	14
48533.780.....	−88	15
48534.790.....	−153	13
48535.772.....	−202	13
48537.777.....	−190	13
48538.760.....	−144	12
48539.767.....	−144	13
48540.789.....	−122	20
48542.788.....	−241	15
48543.783.....	−204	15
48895.795.....	−105	10
48897.794.....	−139	11
48898.783.....	−93	11
48899.775.....	−2	11
48900.773.....	−7	10
48901.810.....	−144	11
48902.761.....	−159	7
48903.783.....	−193	10
48904.780.....	−135	11
49199.874.....	212	12
49201.013.....	100	12
49209.846.....	133	11
49212.868.....	157	10
49213.875.....	111	10
49214.874.....	27	10
49216.880.....	203	10
49217.882.....	294	10
49218.874.....	174	10
49219.892.....	152	8
49220.880.....	189	9
49221.857.....	204	9
49222.926.....	277	10
49223.854.....	186	9
49224.888.....	169	10
49225.868.....	242	11
49255.672.....	258	16
49264.815.....	335	12
49268.842.....	320	12
49277.845.....	247	14
49278.839.....	280	13
49279.791.....	275	12
49280.836.....	121	13
49566.867.....	−51	10
49567.842.....	0	10
49568.824.....	0	11
49569.815.....	−12	11
49570.828.....	5	11
49571.863.....	−11	10
49572.835.....	8	11
49573.803.....	−50	10
49574.840.....	−9	10
49575.804.....	−63	11
49576.836.....	−55	10
49601.809.....	41	10
49863.989.....	34	7
49865.958.....	−5	5
49893.990.....	115	7
49941.749.....	166	8
50014.691.....	−10	4
50015.702.....	43	5
50016.725.....	165	5
50017.783.....	208	5
50018.725.....	161	5
50019.691.....	97	4
50020.699.....	102	5

TABLE 17

HR 8313 Measured Doppler Velocities

MJ	Velocity (m s^{-1})	Error (m s^{-1})
48484.930.....	0	16
48485.941.....	19	14
48487.869.....	−2	15
48488.823.....	−66	14
48531.878.....	−122	17
48532.830.....	−61	16
48533.803.....	−39	16
48534.813.....	−91	14
48537.799.....	70	15
48538.782.....	−124	14
48539.788.....	−144	16
48542.809.....	−69	18
48543.804.....	−50	17
48895.816.....	−132	11
48897.811.....	64	12
48898.802.....	83	12
48899.794.....	39	12
48900.790.....	104	12
48901.827.....	−18	13
48902.787.....	54	14
48903.797.....	78	14
48904.802.....	104	9
49199.902.....	53	5
49212.885.....	−94	13
49213.892.....	15	12
49214.891.....	−13	12
49216.921.....	−54	12
49217.898.....	−2	10
49218.886.....	43	12
49219.910.....	−43	11
49220.896.....	30	11
49221.878.....	31	12
49222.938.....	6	11
49223.872.....	−80	10
49224.904.....	−96	11
49225.884.....	−178	11
49268.858.....	−293	15
49277.861.....	−135	13
49278.857.....	−97	13
49279.808.....	−142	14
49280.853.....	−141	13
49566.880.....	18	15
49567.853.....	−5	16
49568.836.....	77	13
49569.826.....	−3	13
49570.838.....	−5	17
49571.873.....	18	14
49572.846.....	−67	15
49573.814.....	52	13
49574.849.....	26	12
49866.888.....	66	7
50014.761.....	67	7

motion is unlikely to be the cause of the observed velocity variations. The mass of a companion that induces an amplitude of $\sim$100 m s^{-1} and a period of 230 days or less, consistent with most of the stars in this sample, would be less than 10 $M_{\rm JUP}$. While it is possible that the observed velocity variations are caused by orbiting planetary mass companions, the data is not compelling. Sinusoidal and Keplerian fits to the observed velocities typically reduce the scatter of the observed velocities by less than a factor of 2. Thus an orbital hypothesis would still require intrinsic stellar variations with an amplitude of the same order (or larger) than the variations resulting from orbital reflex motion. This is also true of the two stars (HR 7796 and HR 7387) that have larger velocity amplitudes. In addition, only

TABLE 18

HR 8414 MEASURED DOPPLER VELOCITIES

MJD	Velocity (m s^{-1})	Error (m s^{-1})
48117.956.....	12	26
48119.927.....	−1	20
48120.851.....	−27	24
48121.849.....	−36	22
48123.887.....	35	22
48124.870.....	−68	23
48125.885.....	−77	22
48126.895.....	−27	23
48127.944.....	55	25
48130.940.....	51	21
48131.845.....	24	21
48132.885.....	84	22
48133.978.....	116	22
48134.974.....	85	21
48135.902.....	−39	19
48484.955.....	−338	16
48485.960.....	−245	22
48487.935.....	−75	16
48488.847.....	−319	11
48531.902.....	125	28
48532.857.....	154	14
48533.826.....	193	13
48534.836.....	79	12
48537.819.....	95	12
48538.803.....	59	11
48539.808.....	31	13
48540.818.....	41	12
48542.829.....	51	14
48543.824.....	21	13
48894.820.....	74	16
48895.835.....	123	11
48897.827.....	64	12
48898.824.....	27	11
48899.814.....	−45	11
48900.808.....	38	11
48901.858.....	3	8
48902.801.....	−75	12
48903.810.....	−73	11
48904.851.....	−15	16
49199.923.....	−198	10
49212.904.....	−78	12
49213.908.....	−45	10
49214.910.....	−6	9
49216.905.....	8	9
49217.915.....	71	11
49218.903.....	29	9
49219.927.....	0	10
49220.916.....	−78	10
49221.897.....	112	9
49222.952.....	106	11
49223.889.....	95	11
49224.921.....	16	9
49225.898.....	79	11
49264.839.....	56	12
49268.874.....	108	13
49277.878.....	136	12
49278.873.....	91	12
49279.824.....	68	12
49280.871.....	28	12
49566.894.....	−155	13
49567.863.....	−148	13
49568.847.....	−194	13
49569.837.....	−125	12
49570.848.....	−13	12
49571.885.....	−33	9
49572.859.....	−129	9
49573.824.....	−119	10
49574.860.....	−124	9
49862.987.....	−79	7
49866.982.....	−46	6

TABLE 18—*Continued*

MJD	Velocity (m s^{-1})	Error (m s^{-1})
50014.783.....	−103	4
50015.715.....	−133	5
50016.734.....	−217	5
50017.795.....	−93	5
50018.738.....	−129	5
50019.707.....	−129	4
50020.711.....	−134	5
50305.837.....	−155	6
50307.880.....	−258	7
50308.769.....	−334	7
50309.858.....	−301	7
50310.841.....	−271	6
50311.831.....	−224	6
50373.786.....	−93	5
50376.815.....	5	6
50377.769.....	−59	5

$\sim$5% of late F and G main-sequence stars have planets that can be detected from Doppler monitoring with a precision of 15 m s^{-1} (Butler & Marcy 1997). Assuming the rate of planet formation in 5 $M_\odot$ stars is not appreciably greater than that of 1 $M_\odot$ stars, it would be expected that at most only one of the program stars would have a detectable planet.

Hatzes & Cochran (1995) have discussed more plausible physical models to account for the observed Doppler veloc-

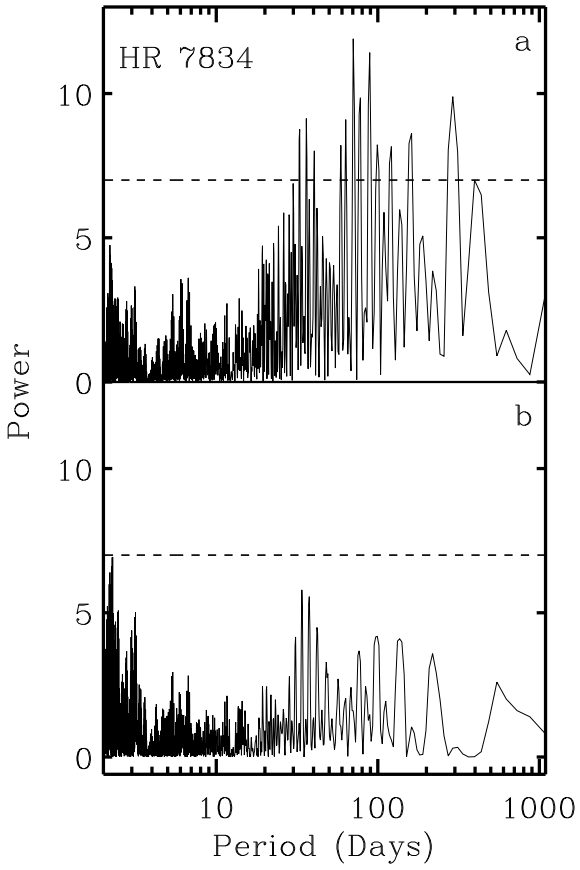

FIG. 36.—Periodogram of HR 7834 velocities. (*a*) Periodogram of measured velocities. The highest periodogram peak has a period of 70.674 days. The 1% false alarm level is indicated by the dotted line. (*b*) Periodogram of residual velocities, after subtracting a best-fit sinusoid with a period of 70.674 days.

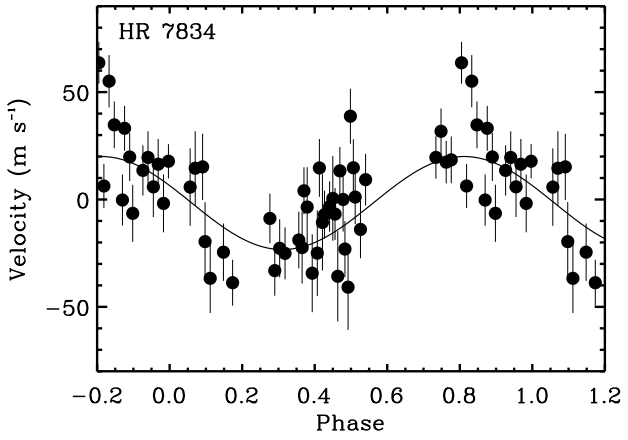

FIG. 37.—HR 7834 Doppler velocities phased with a 70.674 day period. The rms of the sinusoidal fit is 17.5 m s^{-1}.

ity variations of supergiants near the instability strip. Such models include rotational modulation of surface features and nonradial pulsations. Supergiants typically have rotation periods of several hundred days (Rao et al. 1993; Brosius, Mullan, & Stencel 1985)—somewhat longer than the periodicities observed in the Doppler velocities. Dark spots or other surface features modulated by the stellar rotation could produce velocity variations consistent with the observed results. For a star with $v \sin i \sim 17$ km s^{-1}, a dark spot would have to cover approximately 0.6% of the surface to account for 100 m s^{-1} velocity variations. The expected photometric variations in this scenario would be 0.06 mag, which is about a factor of 2 larger than the reported variations (Fernie & Hube 1971; Fernie 1976). Spot coverage would have to be correspondingly larger for stars with smaller values of $v \sin i$. Both the nonradial pulsations and the rotating spot models would be expected to produce multiple periodicities.

Rao et al. (1993) have monitored Ca II H and K emission in a handful of supergiants over 6 yr. All of the stars in this program show multiple periodicities, typically from 50 to 1000 days. Four stars in the H and K program are also included in the current study. HR 8232 showed periodicities in H and K emission ranging from 65 to 1000 days. During the 1987–1988 observing season, the dominant periodicity

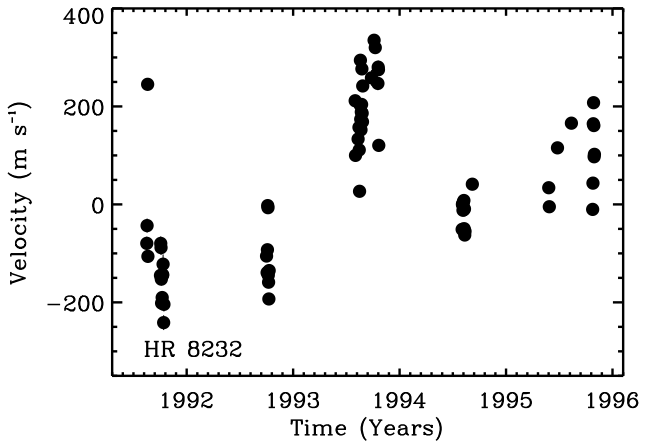

FIG. 38.—Measured Doppler velocities for HR 8232. A total of 70 observations span 4.2 yr. The rms is 155 m s^{-1}, and the full amplitude of the velocity variation is ~500 m s^{-1}.

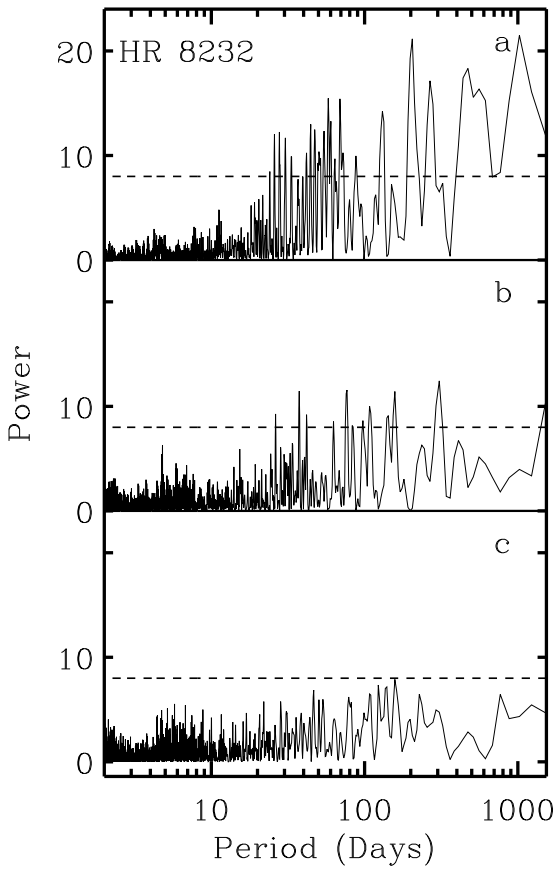

FIG. 39.—Periodogram of HR 8232 velocities. (*a*) Periodogram of measured velocities. The two highest periodogram peaks have periodicities of 1023.866 and 203.417 days. The 1% false alarm level is indicated by the dotted line. (*b*) Periodogram of residual velocities, after subtracting a best-fit sinusoid with a period of 1023.866 days. (*c*) Periodogram of residual velocities, after subtracting a best-fit sinusoid with a period of 203.417 days.

was 223 days, similar to the 203 day periodicity observed in the Doppler velocity measurements. HR 8313 showed a weak H and K periodicity of 476 days, almost exactly twice the length of the 231 day periodicity observed in the

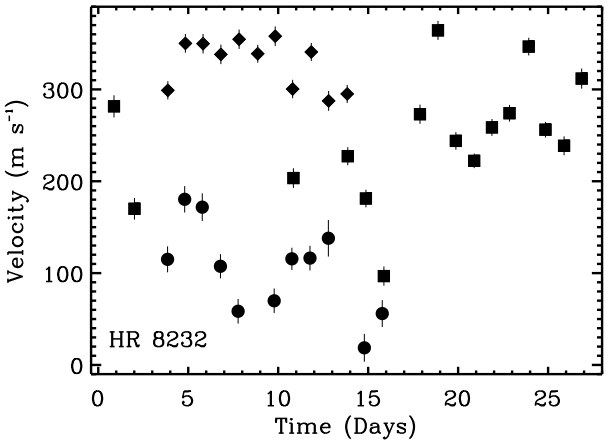

FIG. 40.—Nightly velocity variations of HR 8232 from three observing runs. The velocity zero point of each of these runs is arbitrary. *Circles:* Observing run that began in 1991 early October; *squares:* observing run that began in 1993 early August; *diamonds:* observing run that began in 1994 early August. Velocity variations within a single run are typically ~100 m s^{-1}.

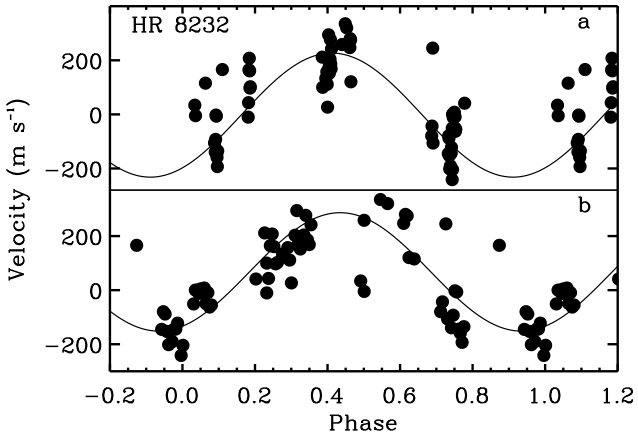

FIG. 41.—Phased Doppler velocities for HR 8232. (*a*) Doppler velocities phased with 1023.866 day period. The rms to the sinusoidal fit is 100 m s^{-1}. (*b*) Doppler velocities phased with a 203.417 day period. The rms to the sinusoidal fit is 99 m s^{-1}.

Doppler velocities. Periodicities in H and K emission for HR 8414 ranged from 97 to 1800 days, compared to the dominant 76 day periodicity in the Doppler velocities. HR 6536 produced weak H and K periodicities of 28 and 42 days, which is similar to the 21 day periodicity from the Doppler velocity measurements.

Evans (1993, Fig. 3) reports little overlap in the H-R diagram between Cepheids and nonvariable supergiants, with the bulk of the nonvariable stars being systematically redder and less luminous than the Cepheids. The nonvariables would thus occupy the region between Fernie's (1990) restricted red edge of the instability strip and the traditional red edge. This is somewhat inconsistent with Figure 1 of this paper, which shows the program stars distributed throughout the region of the instability strip, including several within the restricted instability strip. While the $B-V$ values for the stars in Figure 1 are precisely known, the absolute luminosities have simply been estimated from the spectral class, and could reasonably be inaccurate by a magnitude or more. Assuming that the errors in the estimate of absolute luminosity are not systematically much larger than 1 mag, Figure 1 suggests that that the nonvariable supergiants are not excluded from the restricted Cepheid instability strip.

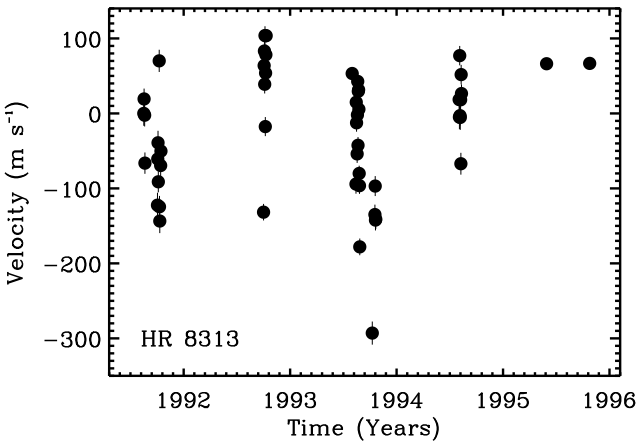

FIG. 42.—Measured Doppler velocities for HR 8313. A total of 52 observations span 4.2 yr. The rms is 84 m s^{-1}, and the full amplitude of the velocity variation is ~400 m s^{-1}.

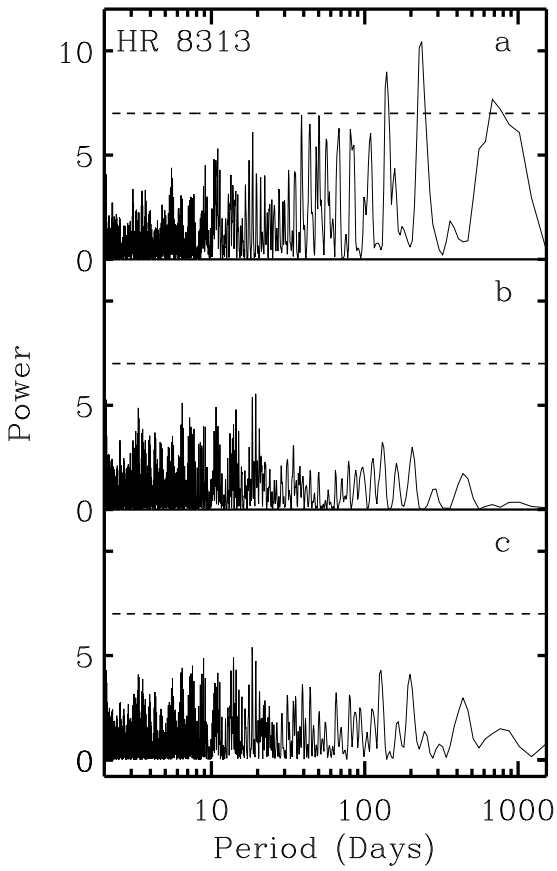

FIG. 43.—Periodogram of HR 8313 velocities. (*a*) Periodogram of measured velocities. The two highest periodogram peaks have periodicities of 230.918, 137.823, and 711.549 days. The 1% false alarm level is indicated by the dotted line. (*b*) Periodogram of residual velocities, after subtracting a best-fit sinusoid with a period of 230.918 days. (*c*) Periodogram of residual velocities, after subtracting a best-fit sinusoid with a period of 137.823 days.

As Figure 49 demonstrates, the program stars are spectroscopically very similar to δ Cep. There are no obvious differences that might be attributed to rotation or abundances. The one notable difference, the width of the Balmer

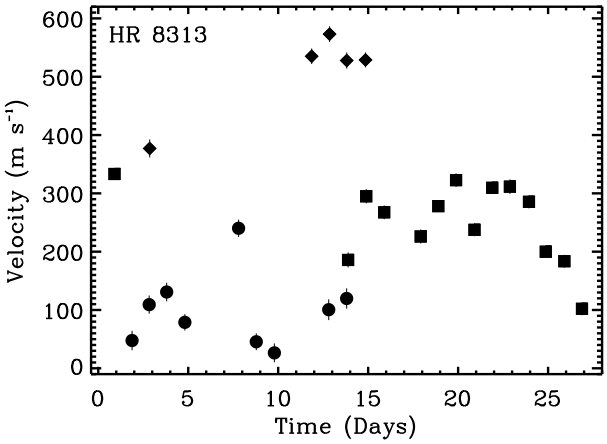

FIG. 44.—Nightly velocity variations of HR 8313 from three observing runs. The velocity zero point of each of these runs is arbitrary. *Circles:* Observing run that began in 1991 early October; *squares:* observing run that began in 1993 late July; *diamonds:* observing run that began in 1993 early October. Velocity variations within a single run are typically ~200 m s^{-1}.

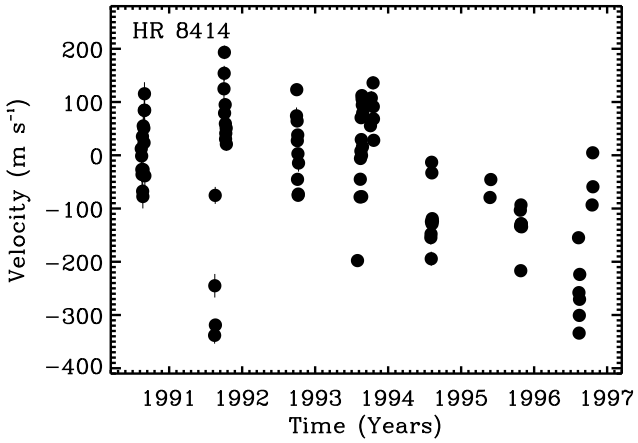

FIG. 45.—Measured Doppler velocities for HR 8414. A total of 86 observations span 6.2 yr. The rms is 123 m s^{-1}, and the full amplitude of the velocity variation is $\sim$500 m s^{-1}.

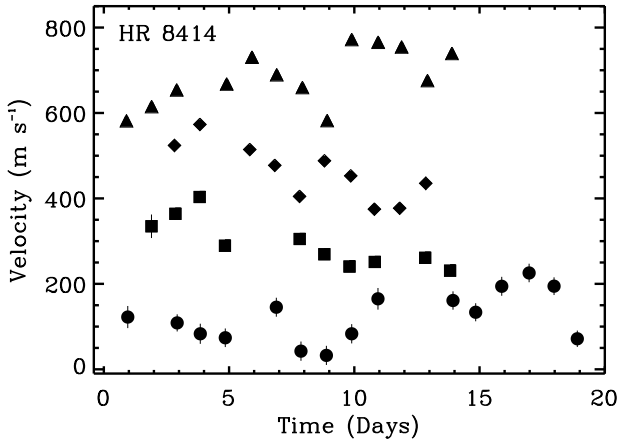

FIG. 47.—Nightly velocity variations of HR 8414 from four observing runs. The velocity zero point of each of these runs is arbitrary. *Circles:* observing run that began in 1990 mid-August; *squares:* observing run that began in 1991 early October; *diamonds:* observing run that began in 1992 late September; *triangles:* observing run that began in 1993 mid-August. Velocity variations within a single run are typically $\sim$150 m s^{-1}.

lines, suggests greater chromospheric activity in the non-Cepheids, consistent with the far-UV observations of Evans & Teays (1996) and the X-ray observations of Sasselov & Sabbey (1994). The excess chromospheric activity in the non-Cepheids is diagnostic, but it does not explain why the two classes of stars differ.

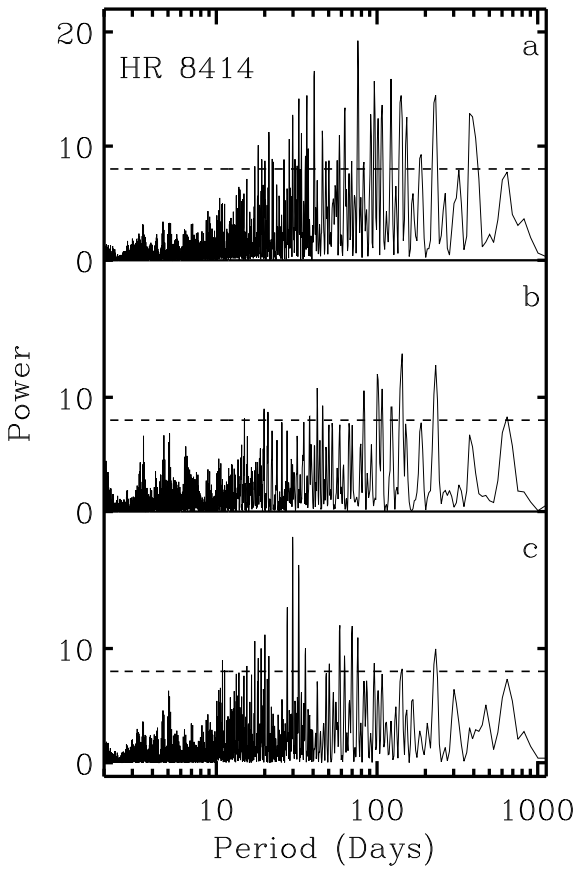

FIG. 46.—Periodogram of HR 8414 velocities. (*a*) Periodogram of measured velocities. The three highest periodogram peaks have periodicities of 76.152, 40.626, and 121.987 days. The 1% false alarm level is indicated by the dotted line. (*b*) Periodogram of residual velocities, after subtracting a best-fit sinusoid with a period of 76.152 days. (*c*) Periodogram of residual velocities, after subtracting a best-fit sinusoid with a period of 40.626 days.

The questions remain of what sets the pulsation amplitudes of Cepheids, and what is causing the odd behavior of the "stable" stars in the Cepheid instability strip? In one of the earliest papers that addressed this issue, Schmidt (1972) concludes, "It appears premature to compare the theoretical location of the instability zone with observation until the occurrence of nonvariables in that region is better understood." Though a quarter of a century has passed, this problem still stands.

Geoffrey W. Marcy and Roger A. Bell have given a great deal of helpful advice over the many years that this project has spanned. Nancy Evans made several useful comments about an early draft of this paper. This work has received generous supported from the NSF (AST 95-20443), SUN Microsystems, and NASA (NAGW 3182). This research has made use of the Simbad database, operated at CDS, Strasbourg, France.

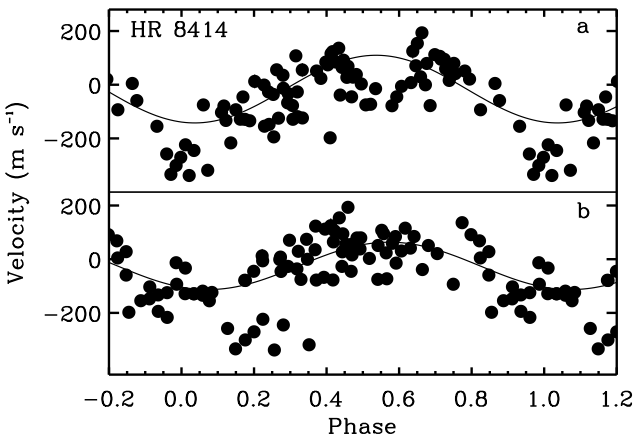

FIG. 48.—Phased Doppler velocities for HR 8414. (*a*) Doppler velocities phased with 76.152 day period. The rms to the sinusoidal fit is 87 m s^{-1}. (*b*) Doppler velocities phased with a 40.626 day period. The rms to the sinusoidal fit is 93 m s^{-1}.

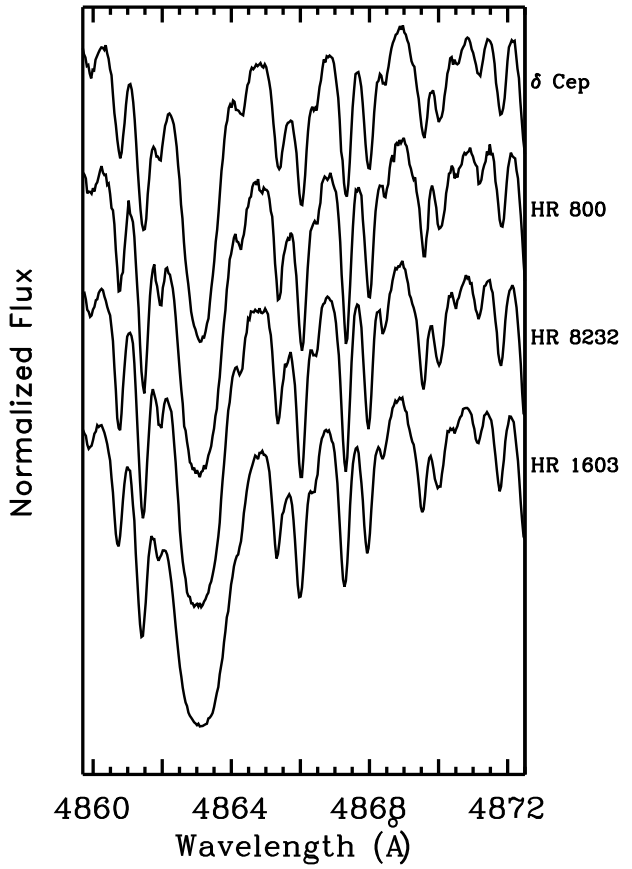

FIG. 49.—Line profiles around Hβ of G0 supergiants, compared to δ Cep. The spectrum of δ Cep was taken from phase 0.66 so as to match the $B-V$ of G0 stars. The Hβ line in δ Cep is narrower than that of the 3 G0 supergiants, but the spectra are otherwise quite similar both in line strengths and widths.

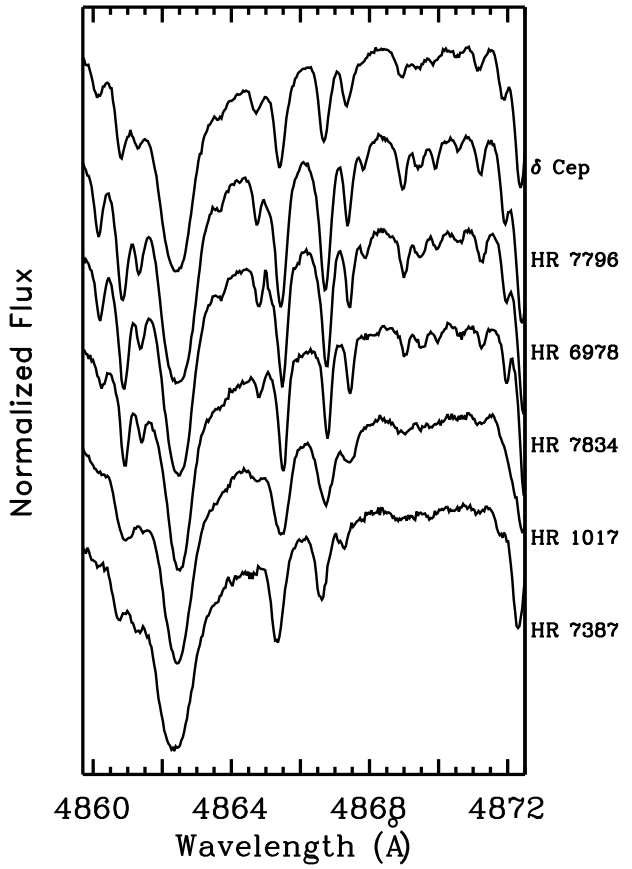

FIG. 50.—Line profiles around Hβ of F supergiants, compared to δ Cep. The spectrum of δ Cep was taken from phase 0.07 so as to match approximately the $B-V$ of F supergiants. The spectra of the late F supergiants are similar to δ Cep.

REFERENCES

Berseir, D. 1996, A&A, 308, 514
Brosius, J. W., Mullan, D. J., & Stencel, R. E. 1985, ApJ, 288, 310
Burki, G., & Mayor, M. 1983, A&A, 124, 256
Butler, R. P. 1992, ApJ, 394, L25
———. 1993, ApJ, 415, 323
Butler, R. P., & Marcy, G. W. 1996, ApJ, 464, L153
———. 1997, in Proc. Int. Workshop Brown Dwarfs and Extrasolar Planets, ed. R. Rebolo, E. L. Martin, & M. R. Zapatero-Osorio (San Francisco: ASP), in press
Butler, R. P., Marcy, G. W., Williams, E., McCarthy, C., Dosanjh, P., & Vogt, S. S. 1996, PASP, 108, 500
Chiosi, C., Wood, P., Bertelli, G., & Bressan, A. 1992, ApJ, 387, 320
Evans, N. R. 1993, AJ, 105, 1956
Evans, N. R., Jiang, J. H., McAlary, C. W., & Campins, H. 1993, AJ, 106, 726
Evans, N. R. & Teays, T. J. 1996, AJ, 112, 761
Evans, N. R., Teays, T. J., Taylor, L. L., Lester, J. B., & Hindsley, R. B. 1996, AJ, 111, 2099
Fernie, J. D. 1976, PASP, 88, 116
———. 1990, ApJ, 354, 295
Fernie, J. D., & Hube, J. O. 1971, ApJ, 168, 437
Gilliland, R. L., & Baliunas, S. L. 1987, ApJ, 314, 766
Hatzes, A. P., & Cochran, W. D. 1993, ApJ, 413, 339
Hatzes, A. P., & Cochran, W. D. 1994, ApJ, 432, 763
———. 1995, ApJ, 452, 401
Hoffleit, D., & Jaschek, C. 1982, Yale Bright Star Catalogue (4th ed.; New Haven: Yale Univ. Press)
Larson, A. M., Irwin, A. W., Yang, S. L. S., Goodenough, C., Walker, G. A. H., Walker, A. R., & Bohlender, D. A. 1993, PASP, 105, 825
Marcy, G. W., & Butler, R. P. 1992, PASP, 104, 270.
———. 1996, ApJ, 464, L147
Murdoch, K. A., Hearnshaw, J. B., & Clark, M. 1993, ApJ, 413, 349
Percy, J. R. 1975, Inf. Bull. Var. Stars, 983
Percy, J. R., Baskerville, I., & Trevorrow, D. W. 1979, PASP, 91, 368
Rao, L. M., Baliunas, S. L., Robinson, C. R., Frazer, J., Woodard, L., & Donahue, R. A. 1993, in ASP Conf. Ser. 45, Ca II H and K Variations of a Sample of Hybrid Stars: Do Hybrids Pulsate? ed. D. Sasselov (San Francisco: ASP), 300
Sasselov, D. D., & Sabbey, C. N. 1994, Rev. Mexicana Astron. Af., 29, 215
Scargle, J. D. 1982, ApJ, 263, 835
Schmidt, E. G. 1972, ApJ, 172, 679
Smith, P. H., McMillan, R. S., & Merline, W. J. 1987, ApJ, 317, L79
Valenti, J. A., Butler, R. P., & Marcy, G. W. 1995, PASP, 107, 966
Vogt, S. S. 1987, PASP, 99, 1214
Walker, G. A. H., Yang, S., Campbell, B., & Irwin, A. W. 1989, ApJ, 343, L21